

Towards a Theoretical Understanding of the ‘Reversal Curse’ via Training Dynamics

Hanlin Zhu^{*1,2} Baihe Huang^{*1} Shaolun Zhang¹ Michael Jordan¹
 Jiantao Jiao¹ Yuandong Tian² Stuart Russell¹

¹UC Berkeley ²Meta AI

{hanlinzhu,baihe_huang,shaolun_zhang,jiantao}@berkeley.edu
 {jordan,russell}@cs.berkeley.edu
 yuandong@meta.com

May 11, 2024

Abstract

Auto-regressive large language models (LLMs) show impressive capacities to solve many complex reasoning tasks while struggling with some simple logical reasoning tasks such as inverse search: when trained on “A is B”, LLM fails to directly conclude “B is A” during inference, which is known as the “reversal curse” (Berglund et al., 2023). In this paper, we theoretically analyze the reversal curse via the training dynamics of (stochastic) gradient descent for two auto-regressive models: (1) a bilinear model that can be viewed as a simplification of a one-layer transformer; (2) one-layer transformers using the framework of Tian et al. (2023a). Our analysis reveals a core reason why the reversal curse happens: the (effective) weights of both auto-regressive models show *asymmetry*, i.e., the increase of weights from a token A to token B during training does not necessarily cause the increase of the weights from B to A . Moreover, our analysis can be naturally applied to other logical reasoning tasks such as chain-of-thought (COT) (Wei et al., 2022b). We show the necessity of COT, i.e., a model trained on “ $A \rightarrow B$ ” and “ $B \rightarrow C$ ” fails to directly conclude “ $A \rightarrow C$ ” without COT (also empirically observed by Allen-Zhu and Li (2023)), for one-layer transformers via training dynamics, which provides a new perspective different from previous work (Feng et al., 2024) that focuses on expressivity. Finally, we also conduct experiments to validate our theory on multi-layer transformers under different settings.

1 Introductions

Large language models (LLMs) have shown great performance in solving complex reasoning tasks that require multiple reasoning steps through in-context learning (ICL), such as zero-shot learning (Reynolds and McDonell, 2021; Kojima et al., 2022), few-shot learning (Brown et al., 2020; Wei et al., 2022b; Wang et al., 2022), or via further fine-tuning (Nye et al., 2021; Cobbe et al., 2021; Zelikman et al., 2022). However, without the above inference-time techniques or model fine-tuning (probably combined with data manipulations), an auto-regressive LLM might struggle with simple logical reasoning tasks that require multiple reasoning steps learned during training separately or

*equal contributions.

require simple manipulation of the learned knowledge (Allen-Zhu and Li, 2023), where the reversal curse (Berglund et al., 2023) serves as a well-known example.

Reversal curse (Berglund et al., 2023) refers to the phenomenon that an auto-regressive LLM that learns “A is B” during training fails to generalize to the reverse direction “B is A”, and this task is also termed as “inverse search” in Allen-Zhu and Li (2023). Although some previous works propose different methods to mitigate the reversal curse, including reversing the training dataset (Guo et al., 2024; Golovneva et al., 2024) and training on different objectives such as autoregressive blank infilling (Lv et al., 2023), these methods might negatively affect the model performance on other tasks since they either alter the dataset or the model architecture. Without dataset manipulation or changing the auto-regressive nature (causal structure) of the model, the reversal curse is hard to mitigate even with ICL strategies such as chain-of-thought (Allen-Zhu and Li, 2023; Guo et al., 2024).

In this paper, we aim to theoretically study why the reversal curse happens for auto-regressive LLMs. Different from previous work that studies the capacity of (transformer-based (Vaswani et al., 2017)) LLMs through the lens of expressivity (e.g., Yun et al. (2019); Pérez et al. (2021); Feng et al. (2024)), reversal curse cannot be explained by expressivity since a model can express “A is B” is also able to express “B is A”. Therefore, we analyze the reversal curse via training dynamics since even if a set of parameters can express a fact in both directions, it might not be reachable through popular training algorithms (e.g., gradient descent, AdamW (Loshchilov and Hutter, 2017)) with training data only presented in one direction. We summarize our main contributions as follows:

- We theoretically analyze reversal curse where training or test sequences have the form “ $A \rightarrow B$ ” or “ $B \leftarrow A$ ” via training dynamics of (stochastic) gradient descent under two auto-regressive models: a bilinear model (Section 3) and one-layer transformers under certain assumptions similar to Tian et al. (2023a) (Section 4). The analysis of the training dynamics of both models reveals a core reason why the reversal curse happens: the weights of the autoregressive models are *asymmetric*, i.e., the increase of weights from the token A to token B ¹ during training does not necessarily cause the increase of the weights from B to A . We emphasize that during theoretical analysis, we used reparameterization. Thus, the weights from A to B do not necessarily correspond to the actual model weights and should be viewed as effective weights. For the bilinear model, the weight from A to B is $\mathbf{u}_A^\top \Theta \mathbf{u}_B$ for embeddings $\mathbf{u}_A, \mathbf{u}_B$ and parameter matrix Θ ; in our analysis for one-layer transformers, the weight from A to B is Y_{AB} where Y is a matrix of parameters (after re-parameterization); empirically, the weight from A to B is the logits of B when the input is A . Although the (effective) weights from A to B and from B to A might be related to some extent since they are both computed using the same set of embeddings, their correlation is weak and thus show asymmetry as verified both theoretically (Sections 3 and 4) and empirically (Section 5).
- The techniques we used to analyze the reversal curse can be applied to other logical reasoning tasks. In particular, we use the above framework to show the necessity of chain-of-thought (COT) (Wei et al., 2022b) (i.e., a model trained on “A implies B” and “B implies C” separately struggles to directly conclude “A implies C” without COT, which was also empirically observed by Allen-Zhu and Li (2023)) via training dynamics of one-layer transformers (Section 4.2), which provides a new perspective different from previous work Feng et al. (2024) that focuses on the expressivity of transformers. Slightly different from the reason for the reversal curse, in COT analysis, the model weights show *intransitivity*, i.e., increasing the weights from the

¹The weights from A to B can be viewed as the logits of token B when the input is A .

token A to B and B to C does not necessarily increase the weights from A to C . We emphasize again that the weights refer to effective weights.

- We also empirically validate our theoretical results through the training dynamics of multi-layer transformers (Section 5).

The *asymmetry* and *intransitivity* of weights of auto-regressive models indicate that auto-regressive LLMs might not automatically deduce indirect conclusions using separate knowledge learned during training: to make a model predicting token B where the input token is A , the model needs to see B following A in the same sequence during the training set due to the next token prediction objective and model architectures. This also highlights the importance of ICL, data augmentation, or planning for LLMs with the current popular causal transformer-based structures to solve complex reasoning tasks.

1.1 Related works

LLM Reasoning. The strong performance of LLMs on reasoning tasks (Brown et al., 2020; Cobbe et al., 2021; Huang et al., 2022; Kojima et al., 2022; Jung et al., 2022; Wei et al., 2022b; Han et al., 2024) has prompt many studies on the reasoning capabilities of LLMs. Xie et al. (2021) argues that transformers perform implicit Bayesian inference in ICL. Olsson et al. (2022) shows that transformers implement a specific type of circuits called “induction heads” that are key to the ICL abilities of LLMs. Nichani et al. (2024) proves that causal structures are encoded in transformer layers during the training dynamics. Brinkmann et al. (2024) identifies a backward chaining mechanism of transformers in deductive reasoning. Apart from in-context reasoning, LLMs still demonstrate limitations in other types of reasoning tasks (Valmeekam et al., 2022; Chang et al., 2023; Zhang et al., 2024).

Reversal Curse. Berglund et al. (2023) identifies the phenomenon of reversal curse. This drawback of LLMs is also demonstrated in Qi et al. (2023). Allen-Zhu and Li (2023) studies a similar phenomenon in which LLMs face difficulty in manipulating already learned knowledge. Several paper studies eliminating the reversal curse by extending causal attention to bidirectional attention (Lv et al., 2023), training on reversed samples (Golovneva et al., 2024), permuting semantic units (Guo et al., 2024), or introducing reverse logic data (Luo et al., 2024). Given all the empirical works, theoretical analysis of the reversal curse phenomenon remains scarce.

Expressivity of LLMs. There is a long line of works (Yun et al., 2019; Bhattamishra et al., 2020a,b; Dehghani et al., 2018; Pérez et al., 2021; Edelman et al., 2022; Elhage et al., 2021; Likhoshervstov et al., 2021; Akyürek et al., 2022; Zhao et al., 2023; Yao et al., 2021; Anil et al., 2022; Barak et al., 2022; Garg et al., 2022; Von Oswald et al., 2022; Bai et al., 2023; Olsson et al., 2022; Akyürek et al., 2022; Li et al., 2023) studying the behavior of LLMs through the expressivity of transformers. It has been shown that transformers can implement simple functions such as sparse linear functions, two-layer neural networks, and decision trees (Garg et al., 2022), gradient descent (Akyürek et al., 2022; Bai et al., 2023; Von Oswald et al., 2023), automata (Liu et al., 2022), Turing machines (Wei et al., 2022a), variational inference (Mei and Wu, 2023), and bandit algorithms (Lin et al., 2023). However, the reversal curse cannot be explained through expressivity since an LLM with the power to express a fact in one direction naturally has the power to express it in the other.

Training dynamics of LLMs. There are rich literatures in the optimization of attention layers (Zhang et al., 2020; Hron et al., 2020; Yang et al., 2022; Boix-Adsera et al., 2023; Bietti et al., 2023; Jelassi et al., 2022; Snell et al., 2021). Mahankali et al. (2023); Zhang et al. (2023) study the dynamics of a single linear attention layer in in-context linear regression. Fu et al. (2024) proves convergence of one-layer transformers in random feature regime. Huang et al. (2023) shows the convergence of gradient descent on one-layer transformers in in-context linear regression with orthogonal data. Tian et al. (2023a) studies the convergence of one-layer transformers in a class of next-token prediction tasks. Tian et al. (2023b) studies training dynamics of multi-layer transformers. Nichani et al. (2024) studies gradient descent on a class of two-layer transformers in in-context learning tasks with latent causal structures. Our paper studies the reversal curse via training dynamics under both bilinear settings and one-layer transformers. For one-layer transformers, we use the same framework as Tian et al. (2023a) without the need for certain technical assumptions such as long input sequences, different learning rates for different parameters, or weak correlations that are required for Tian et al. (2023a). Besides, we focus on the generalization ability of models for logical reasoning tasks while Tian et al. (2023a) mainly focus on optimization, and we identify the asymmetry and intransitivity properties of model weights, which are the core reasons for the failure of LLM for certain types of logical reasoning. Moreover, our analysis of the bilinear model only requires the embedding to be almost orthonormal, while Tian et al. (2023a) essentially assumed the embedding vectors to be fixed and one-hot.

2 Preliminaries

Basic notations. For any integer $N > 0$, we use $[N]$ to denote the set $\{1, 2, \dots, N\}$. Let \mathbb{R}, \mathbb{N} denote the set of real numbers and natural numbers, respectively. For real variables x_1, \dots, x_n , we use $\text{poly}(x_1, \dots, x_n)$ to denote the polynomial of x_1, \dots, x_n . Let $\delta_{ij} = 1$ for $i = j$ and $\delta_{ij} = 0$ for $i \neq j$. We use $f(n) \lesssim g(n)$ if there exists a constant $C > 0$ s.t. $f(n) \leq Cg(n), \forall n$; we say $g(n) \gtrsim f(n)$ if $f(n) \lesssim g(n)$.

Without further specification, all vectors in this paper are column vectors by default. For a squared matrix $A \in \mathbb{R}^{d \times d}$, its trace is $\text{Tr}(A) = \sum_{i=1}^d A_{ii}$. For two matrices $A, B \in \mathbb{R}^{m \times n}$ of the same shape, their inner product is defined as $\langle A, B \rangle = \text{Tr}(AB^\top)$. For any matrix $A \in \mathbb{R}^{m \times n}$, its (Frobenius) norm is defined as $\|A\| = \sqrt{\langle A, A \rangle}$. For any vector $\mathbf{x} = (x_1, \dots, x_d)^\top \in \mathbb{R}^d$ or a matrix $A \in \mathbb{R}^{m \times n}$, we define the zero-norm as $\|\mathbf{x}\|_0 = \sum_{i=1}^d \mathbb{1}\{x_i \neq 0\}$ or $\|A\|_0 = \sum_{i=1}^m \sum_{j=1}^n \mathbb{1}\{A_{ij} \neq 0\}$ where $\mathbb{1}\{\cdot\}$ is the indicator function. We use \mathbf{e}_i to denote one-hot vectors where only the i -th entry of \mathbf{e}_i equals one and all other entries are zero. We use $\mathbf{1}$ to denote all-one vectors, $\mathbf{0}$ to denote zero vectors or zero matrices, and I to denote the identity matrix. We will also add subscripts when we want to explicitly show the dimension, such as $\mathbf{0}_d, I_d$ for d -dimensional zero vector and $d \times d$ identity matrix. We use \otimes to denote tensor product of vectors or matrices and use $\mathbf{x}^{\otimes 2}$ and $A^{\otimes 2}$ to denote $\mathbf{x} \otimes \mathbf{x}$ and $A \otimes A$ for vector \mathbf{x} and matrix A .

We use $\mathcal{N}(\boldsymbol{\mu}, \Sigma)$ (or adding subscripts such as $\mathcal{N}_d(\cdot, \cdot)$ if we want to show dimensions explicitly) to denote the (multi-variate) Gaussian distribution with mean $\boldsymbol{\mu}$ and covariance Σ . Also, we use $\Delta(\mathcal{X})$ to denote the set of distributions over a set \mathcal{X} and use $\mathbb{E}[\cdot]$ to denote expectation. For any dataset $\mathcal{D} = \{x_1, x_2, \dots, x_n\}$ where $x_i \in \mathcal{X}$ and a function $f : \mathcal{X} \rightarrow \mathbb{R}$, we define the empirical expectation over the dataset as $\mathbb{E}_{\mathcal{D}}[f] = \frac{1}{n} \sum_{i=1}^n f(x_i)$.

Auto-regressive models. Define the vocabulary $\mathcal{V} = [M]$ for a positive integer $M > 0$ which is the size of the vocabulary. Let $x = (x_1, x_2, \dots, x_T)$ be a sequence of tokens of length T where each token $x_t \in \mathcal{V}, \forall t \in [T]$. We study auto-regressive models $p_\theta(\cdot|x) \in \Delta(\mathcal{V})$ parameterized by θ that

take the sequence x as input and predict the distribution of the next token $x_{T+1} \in \mathcal{V}$. For both models that we study in this paper, the next token probability is modeled as the softmax applied to the logits $l_\theta(\cdot|x) \in \mathbb{R}^M$ of each token in the vocabulary, i.e.,

$$p_\theta(y|x) = \frac{\exp(l_\theta(y|x))}{\sum_{v \in \mathcal{V}} \exp(l_\theta(v|x))}, \quad \forall y \in \mathcal{V}. \quad (1)$$

Also, each token $v \in \mathcal{V}$ has a corresponding embedding vector $\mathbf{u}_v \in \mathbb{R}^d$ which might be fixed or learnable. In both [Sections 3](#) and [4](#), each data point in the dataset is a sequence of tokens, i.e., the i -th training sample in the dataset is $x[i] = (x_1[i], x_2[i], \dots, x_{T[i]}[i], x_{T[i]+1}[i])$ of length $T[i] + 1$ where $x_{T[i]+1}[i]$ is the next token to be predicted. We train both models using cross-entropy loss

$$\mathcal{L}(\theta) = E_{\mathcal{D}}[-\log p_\theta(x_{T+1}|x_1, \dots, x_T)]. \quad (2)$$

Notations for different tokens in [Section 4](#). We show notations for different tokens used for [Section 4](#) in [Table 1](#). For the reversal curse, we use two tokens, “ \rightarrow ” and “ \leftarrow ”, to represent forward and backward relationships. For COT, we use “ \rightarrow ” and “ \rightsquigarrow ” to represent direct implication and indirect implication. In [Section 4.3](#), we use $\mathbf{R}_1, \mathbf{R}_2$ to denote the tokens representing relationships. $\mathbf{A}, \mathbf{B}, \mathbf{C}, \mathbf{A}_i, \mathbf{B}_i, \mathbf{C}_i$ are tokens representing entities.

Entities	Forward	Backward	Direct	Indirect	Others
$\mathbf{A}, \mathbf{B}, \mathbf{C}, \mathbf{A}_i, \mathbf{B}_i, \mathbf{C}_i$	\rightarrow	\leftarrow	\rightarrow	\rightsquigarrow	$\mathbf{R}_1, \mathbf{R}_2$

Table 1: Notations for different tokens in [Section 4](#). “ \rightarrow ” and “ \leftarrow ” denote forward and backward relationships for the reversal curse. “ \rightarrow ” and “ \rightsquigarrow ” denote direct implication and indirect implication for COT. \mathbf{R}_1 and \mathbf{R}_2 are two other tokens representing relationships in [Section 4.3](#). $\mathbf{A}, \mathbf{B}, \mathbf{C}, \mathbf{A}_i, \mathbf{B}_i, \mathbf{C}_i$ denote tokens representing entities.

3 Bilinear Model

We start our analysis of the reversal curse with a bilinear model, which can be viewed as a simplification of one-layer transformers with input length one and decoder layer only. Note that in this section, we assume the embeddings of each token are fixed, so we will directly use the embedding vector to represent a token.

Datasets. Assume the vocabulary has size m where each token $v_1, v_2, \dots, v_m \stackrel{i.i.d.}{\sim} \mathcal{N}_d(0_d, \frac{1}{d}I_d)$. Let $\mathcal{V} = \{v_1, \dots, v_m\}$ and let $\mathcal{X} = \{x_1, \dots, x_n\}$ and $\mathcal{Y} = \{y_1, \dots, y_n\}$ be disjoint random subsets of \mathcal{V} . Assume all training and test sequences have a length of two. For any $2 \leq i \leq n$, the training dataset contains both sequence (x_i, y_i) and (y_i, x_i) . In addition, the training set contains (x_1, y_1) while the test set only contain one example (y_1, x_1) . During training, the model learns both (x_i, y_i) and (y_i, x_i) for $i \geq 2$ to conclude that (x_i, y_i) is equivalent to (y_i, x_i) . For example, \mathcal{X} is a set of names and \mathcal{Y} is a set of books. The sequence (x_i, y_i) means “ x_i is the author of y_i ”, and the sentence (y_i, x_i) means “ y_i is written by x_i ”. We test whether the model is able to infer an unseen sequence (y_1, x_1) given the training data which includes the other direction (x_1, y_1) .

Bilinear model. We consider a bilinear model parameterized by $\Theta \in \mathbb{R}^{d \times d}$ of which the input sequence consists of a single token $x \in \mathcal{V}$. The logits of the next token $y \in \mathcal{V}$ is defined as $l_\Theta(y|x) = x^\top \Theta y$ which is bilinear in x and y , and thus the prediction of next token probability is

$$p_\Theta(y|x) = \frac{\exp(l_\Theta(y|x))}{\sum_{v \in \mathcal{V}} \exp(l_\Theta(v|x))}.$$

The training loss function (2) for bilinear model is

$$\mathcal{L}(\Theta) = \frac{1}{2n-1} \left(\sum_{i=1}^n -\log p_\Theta(y_i|x_i) + \sum_{i=2}^n -\log p_\Theta(x_i|y_i) \right)$$

and the test loss (reversal loss) is

$$\mathcal{L}^{\text{rev}}(\Theta) = -\log p_\Theta(x_1|y_1).$$

We study the training dynamics of gradient flow

$$\frac{d\Theta_t}{dt} = -\nabla \mathcal{L}(\Theta_t)$$

with the initialization $\Theta_0 \sim \mathcal{N}(\mathbf{0}^{\otimes 2}, \sigma^2 \cdot I^{\otimes 2})$. The following theorem shows a separation of training loss and reversal loss during training dynamics.

Theorem 1 (Separation of training dynamics (informal statement of [Theorem 5](#))). *Fix arbitrary $\delta, \epsilon \in (0, 1)$. Suppose σ is small and $d \geq \text{poly}(n, m, 1/\epsilon, \log(1/\delta))$. With probability at least $1 - \delta$, we have*

$$\frac{\mathcal{L}^{\text{rev}}(\Theta_t)}{\mathcal{L}^{\text{rev}}(\Theta_0)} \geq \left(\frac{\mathcal{L}(\Theta_t)}{\mathcal{L}(\Theta_0)} \right)^\epsilon, \quad \forall t \geq 0.$$

[Theorem 1](#) shows that the reversal loss is lower bounded by the training loss. Note that for large d and small ϵ close to 0, $\left(\frac{\mathcal{L}(\Theta_t)}{\mathcal{L}(\Theta_0)} \right)^\epsilon$ is close to 1 and thus $\mathcal{L}^{\text{rev}}(\Theta_t) \gtrsim \mathcal{L}^{\text{rev}}(\Theta_0)$ which implies that $p_\Theta(x_1|y_1)$ remains small during training. We summarize the above argument in [Theorem 2](#).

Theorem 2 (Lower bound of reversal loss (informal statement of [Theorem 6](#))). *Fix arbitrary $c > 0$ and $C \leq \log(m/2)$. Suppose σ is small and $d \geq \text{poly}(n, m, \log(1/\delta), \log c, 1/\log C)$. With probability at least $1 - \delta$,*

$$\mathcal{L}^{\text{rev}}(\Theta_\tau) \geq C.$$

where τ denotes the first time such that $\mathcal{L}(\Theta_t) \leq c$.

The proofs of [Theorem 1](#) and [Theorem 2](#) are deferred to [Appendix A](#). [Theorem 2](#) implies that for large d , while the training loss can be trained to be arbitrarily small, the reversal loss remains large. In other words, the model fails to infer an unseen sequence (y_1, x_1) given the training data which includes the other direction (x_1, y_1) .

A core reason that the reversal curse happens on the above bilinear model is that the parameter matrix Θ is asymmetric. Therefore, the logits $l_\Theta(y|x) = x^\top \Theta y$ and $l_\Theta(x|y) = y^\top \Theta x$ are not equal in general. Consider a special case where each v_i is a one-hot vector. Then $l_\Theta(y|x) = x^\top \Theta y = \Theta_{ij}$ and $l_\Theta(x|y) = y^\top \Theta x = \Theta_{ji}$ for $x = e_i, y = e_j$. Training on (x, y) can increase Θ_{ij} but not Θ_{ji} , which means the model does not automatically learn the reversal direction (y, x) . In [Section 4](#), we will show that for one-layer transformers, the reversal curse is mainly caused by the same reason, i.e., the asymmetry of the model weights.

4 One-Layer Transformers

In [Section 3](#), we analyzed the reversal curse under a bilinear model. In this section, we analyze the reversal curse for one-layer transformers in a similar setting to [Tian et al. \(2023a\)](#) via training dynamics. We also extend our analysis to chain-of-thought in [Section 4.2](#).

Basic notations. Let $\mathcal{V} = [M]$ be the vocabulary for a positive integer $M > 0$. For any token $x \in [M]$, we also use the corresponding M -dimensional one-hot vector $\mathbf{x} = \mathbf{e}_x \in \mathbb{R}^M$ to represent it. Let $U = [\mathbf{u}_1, \mathbf{u}_2, \dots, \mathbf{u}_M]^\top \in \mathbb{R}^{M \times d}$ be the embedding matrix, where $\mathbf{u}_x \in \mathbb{R}^d$ is the d -dimensional embedding of token $x \in [M]$. Note that $U^\top \mathbf{x} = \mathbf{u}_x$.

Consider the i -th training sample in the dataset, $x[i] = (x_1[i], x_2[i], \dots, x_{T[i]}[i], x_{T[i]+1}[i])$, which is a sequence of tokens of length $T[i]+1$. Here, $x_{T[i]+1}[i]$ is the next token (or equivalently, the label of the i -th data point) to be predicted, $x_{T[i]}[i]$ is the query token, and $(x_1[i], x_2[i], \dots, x_{T[i]-1}[i])$ are the contextual tokens. For any token $x_t[i]$, we will use the corresponding one-hot vector $\mathbf{x}_t[i] = \mathbf{e}_{x_t[i]} \in \mathbb{R}^M$ to represent it. The contextual token matrix $X[i] = [\mathbf{x}_1[i], \mathbf{x}_2[i], \dots, \mathbf{x}_{T[i]-1}[i]]^\top \in \mathbb{R}^{(T[i]-1) \times M}$ consists of the one-hot vectors for each contextual token. When it is clear from the context, we will omit all i in the notations.

One-layer transformer. Consider the i -th sample in the training dataset (and we omit i in all notations) $x = (x_1, x_2, \dots, x_T, x_{T+1})$. Note that the contextual token matrix $X = [\mathbf{x}_1, \mathbf{x}_2, \dots, \mathbf{x}_{T-1}]^\top$ and by definition, $XU = [\mathbf{u}_{x_1}, \mathbf{u}_{x_2}, \dots, \mathbf{u}_{x_{T-1}}]^\top$ contains the embedding of each contextual token in the sequence. We study one-layer transformers in the same setting as [Tian et al. \(2023a\)](#). In particular, for an input token sequence (x_1, x_2, \dots, x_T) , after the one-layer self-attention, we can obtain

$$\tilde{\mathbf{u}}_T = U^\top \text{LN}(X^\top \mathbf{b}_T), \quad b_{tT} = \frac{\exp(\mathbf{u}_{x_T}^\top W_Q W_K^\top \mathbf{u}_{x_t} / \sqrt{d})}{\sum_{t'=1}^{T-1} \exp(\mathbf{u}_{x_T}^\top W_Q W_K^\top \mathbf{u}_{x_{t'}} / \sqrt{d})}, \quad (3)$$

where $\mathbf{b}_T = [b_{1T}, b_{2T}, \dots, b_{T-1,T}]^\top$ contains attention scores (after softmax) that query token x_T attend to each contextual token², $\text{LN}(\cdot)$ is the ℓ_2 -normalization operator where $\text{LN}(\mathbf{x}) = \mathbf{x} / \|\mathbf{x}\|_2$, and $W_Q, W_K \in \mathbb{R}^{d \times d_k}$ are trainable query and key matrices respectively. The logit of each token $x \in [M]$ is then calculated by a decoder layer, i.e.,

$$l_\theta(x|x_1, x_2, \dots, x_T) = \mathbf{u}_x^\top W_V \tilde{\mathbf{u}}_T, \quad (4)$$

where θ encodes all parameters in the transformer, and $W_V \in \mathbb{R}^{d \times d}$ can be viewed as a reparameterization of value matrix, output matrix, and (other possible) parameters in the decoder layer. Finally, the next token prediction probability is obtained by

$$p_\theta(x|x_1, x_2, \dots, x_T) = \frac{\exp(l_\theta(x|x_1, x_2, \dots, x_T))}{\sum_{x' \in [M]} \exp(l_\theta(x'|x_1, x_2, \dots, x_T))} = \frac{\exp(\mathbf{u}_x^\top W_V \tilde{\mathbf{u}}_T)}{\sum_{x' \in [M]} \exp(\mathbf{u}_{x'}^\top W_V \tilde{\mathbf{u}}_T)}. \quad (5)$$

The training objective is to maximize (the logarithm of) the next token prediction probability over the whole training dataset $\mathcal{D}_{\text{train}}$, i.e.,

$$\max_{U, W_K, W_Q, W_V} J \triangleq \mathbb{E}_{\mathcal{D}_{\text{train}}} [\log p_\theta(x_{T+1}|x_1, \dots, x_T)] = \mathbb{E}_{\mathcal{D}_{\text{train}}} \left[\mathbf{u}_{x_{T+1}}^\top W_V \tilde{\mathbf{u}}_T - \log \sum_{x' \in [M]} \mathbf{u}_{x'}^\top W_V \tilde{\mathbf{u}}_T \right]. \quad (6)$$

²Note that we assume the query token will not attend to itself as in [Tian et al. \(2023a\)](#).

Reparameterization. Similar to Tian et al. (2023a), we define $Y = UW_V^\top U^\top \in \mathbb{R}^{M \times M}$ and $Z = UW_Q W_K^\top U^\top / \sqrt{d} \in \mathbb{R}^{M \times M}$ and are interested in the dynamics of Y and Z . Therefore, the attention score (after softmax) is

$$b_{tT} = \frac{\exp(\mathbf{x}_T^\top Z \mathbf{x}_t)}{\sum_{t'=1}^{T-1} \exp(\mathbf{x}_T^\top Z \mathbf{x}_{t'})}, \quad (7)$$

the logit and next token probability becomes

$$l_\theta(x|x_1, x_2, \dots, x_T) = \mathbf{x}^\top Y^\top \text{LN}(X^\top \mathbf{b}_T), \quad p_\theta(x|x_1, x_2, \dots, x_T) = \frac{\exp(\mathbf{x}^\top Y^\top \text{LN}(X^\top \mathbf{b}_T))}{\sum_{x' \in [M]} \exp(\mathbf{x}'^\top Y^\top \text{LN}(X^\top \mathbf{b}_T))}, \quad (8)$$

and the objective can be written as

$$\max_{Y, Z} J = \mathbb{E}_{\mathcal{D}_{\text{train}}} \left[\mathbf{x}_{T+1}^\top Y^\top \text{LN}(X^\top \mathbf{b}_T) - \log \sum_{x' \in [M]} \mathbf{x}'^\top Y^\top \text{LN}(X^\top \mathbf{b}_T) \right]. \quad (9)$$

Let η_Y, η_Z be the learning rate of matrices Y and Z respectively. Then the gradient of Y and Z can be characterized by the following lemma:

Lemma 1 (Gradient of Y and Z for 1-layer transformer, Lemma 1 of (Tian et al., 2023a)). *The gradient of Y and Z w.r.t. (9) of batch size 1 and learning rate η_Y and η_Z can be written as*

$$\dot{Y} = \eta_Y \text{LN}(X^\top \mathbf{b}_T) (\mathbf{x}_{T+1} - \boldsymbol{\alpha})^\top, \quad \dot{Z} = \eta_Z \mathbf{x}_T (\mathbf{x}_{T+1} - \boldsymbol{\alpha})^\top Y^\top \frac{P_{X^\top \mathbf{b}_T}^\perp}{\|X^\top \mathbf{b}_T\|_2} X^\top \text{diag}(\mathbf{b}_T) X, \quad (10)$$

where $P_{\mathbf{v}}^\perp \triangleq I - \mathbf{v}\mathbf{v}^\top / \|\mathbf{v}\|_2^2$ projects any vector to orthogonal complement of \mathbf{v} , $\boldsymbol{\alpha} = [\alpha_1, \alpha_2, \dots, \alpha_M]^\top \in \mathbb{R}^M$ with $\boldsymbol{\alpha} = \exp(Y^\top \text{LN}(X^\top \mathbf{b}_T)) / \mathbf{1}^\top \exp(Y^\top \text{LN}(X^\top \mathbf{b}_T))$.

Proof. \dot{Y} and \dot{Z} can be obtained through direct calculation. One can refer to Lemma 1 of Tian et al. (2023a) for the proof. \square

4.1 Main results for reversal curse

In this section, we analyze the reversal curse through the case where data points are three-token sentences “A \rightarrow B” or “B \leftarrow A”. For each sentence, A and B are two distinct tokens that represent two entities, and \rightarrow and \leftarrow are two special tokens representing a pair of relationships inverse to each other.

Datasets. Let $N_{\text{train}} > 0$, $N_{\text{test}}^{(1)} > 0$ and $N_{\text{test}}^{(2)} > 0$ be three positive integers and let $N_{\text{total}} = N_{\text{train}} + N_{\text{test}}^{(1)} + N_{\text{test}}^{(2)}$. Let $\mathbf{A}_i, \mathbf{B}_i \in \mathcal{V}, \forall i \in [N_{\text{total}}]$ be $2N_{\text{total}}$ distinct tokens representing distinct entities. Let $\rightarrow, \leftarrow \in \mathcal{V} = [M]$ be two additional different tokens that represent two inverse relationships. Specifically, we have $\mathbf{A}_i \rightarrow \mathbf{B}_i$ and $\mathbf{B}_i \leftarrow \mathbf{A}_i$ for all $i \in [N_{\text{total}}]$. For notation convenience, we define the following three index sets

$$\begin{aligned} \mathcal{I}_{\text{train}} &= \{1, 2, \dots, N_{\text{train}}\}, \\ \mathcal{I}_{\text{test}}^{(1)} &= \{N_{\text{train}} + 1, \dots, N_{\text{train}} + N_{\text{test}}^{(1)}\}, \\ \mathcal{I}_{\text{test}}^{(2)} &= \{N_{\text{train}} + N_{\text{test}}^{(1)} + 1, \dots, N_{\text{train}} + N_{\text{test}}^{(1)} + N_{\text{test}}^{(2)}\}. \end{aligned}$$

The training set $\mathcal{D}_{\text{train}}$ consists of all $\mathbf{A}_i \rightarrow \mathbf{B}_i$ and $\mathbf{B}_i \leftarrow \mathbf{A}_i$ for $i \in \mathcal{I}_{\text{train}}$. In addition, $\mathcal{D}_{\text{train}}$ contains $\mathbf{A}_i \rightarrow \mathbf{B}_i$ for $i \in \mathcal{I}_{\text{test}}^{(1)}$ and $\mathbf{B}_i \leftarrow \mathbf{A}_i$ for $i \in \mathcal{I}_{\text{test}}^{(2)}$. For convenience, we let $N = |\mathcal{D}_{\text{train}}|$ to be the size of the training set. The test set $\mathcal{D}_{\text{test}}$ consists of $\mathbf{B}_i \leftarrow \mathbf{A}_i$ for $i \in \mathcal{I}_{\text{test}}^{(1)}$ and $\mathbf{A}_i \rightarrow \mathbf{B}_i$ for $i \in \mathcal{I}_{\text{test}}^{(2)}$. Under our construction of the dataset, the LLM will learn the relationship between \mathbf{A}_i and \mathbf{B}_i for $i \in \mathcal{I}_{\text{train}}$ in both directions to deduce that \rightarrow is reverse to \leftarrow , and learn the relationship between \mathbf{A}_i and \mathbf{B}_i for $i \in \mathcal{I}_{\text{test}}^{(1)} \cup \mathcal{I}_{\text{test}}^{(2)}$ in one direction and will be tested for another.

We aim to prove through the training dynamics of one-layer transformers that the test probability remains negligible during training. In particular, we are interested in

$$p_\theta(x_3 = \mathbf{A}_i | x_1 = \mathbf{B}_i, x_2 = \leftarrow), \quad i \in \mathcal{I}_{\text{test}}^{(1)}$$

and

$$p_\theta(x_3 = \mathbf{B}_i | x_1 = \mathbf{A}_i, x_2 = \rightarrow), \quad i \in \mathcal{I}_{\text{test}}^{(2)}.$$

We also use $p_\theta(\mathbf{A}_i | \mathbf{B}_i \leftarrow)$ and $p_\theta(\mathbf{B}_i | \mathbf{A}_i \rightarrow)$ to more compactly represent $p_\theta(x_3 = \mathbf{A}_i | x_1 = \mathbf{B}_i, x_2 = \leftarrow)$ and $p_\theta(x_3 = \mathbf{B}_i | x_1 = \mathbf{A}_i, x_2 = \rightarrow)$, respectively.

For convenience, we assume zero-initialization $Y(0) = \mathbf{0}$ and $Z(0) = \mathbf{0}$. This is the same as Tian et al. (2023a) and is reasonable since empirically, Y and Z are usually initialized as inner products of d -dimensional vectors with i.i.d Gaussian entries, and thus are almost zero (Lemma 8 in Appendix A). The following proposition shows the initial train/test probabilities are uniform over the vocabulary \mathcal{V} .

Proposition 4.1 (Initial probability under zero initialization). *Assume the transformer is under zero-initialization $Y(0) = \mathbf{0}$ and $Z(0) = \mathbf{0}$. For any $i \in [N_{\text{total}}]$, we have*

$$p_{\theta(0)}(x_3 = \mathbf{B}_i | x_1 = \mathbf{A}_i, x_2 = \rightarrow) = p_{\theta(0)}(x_3 = \mathbf{A}_i | x_1 = \mathbf{B}_i, x_2 = \leftarrow) = 1/M,$$

where $\theta(0) = (Y(0), Z(0))$.

The proof is deferred to Appendix B.1.1. Proposition 4.1 shows that initially, the probability of predicting any \mathbf{B} (or \mathbf{A} , respectively) given any $\mathbf{A} \rightarrow$ (or $\mathbf{B} \leftarrow$, respectively) as input is uniform over the whole vocabulary. When $Y(0)$ and $Z(0)$ are not exactly $\mathbf{0}$ but close to $\mathbf{0}$, the initial prediction will still be close to the uniform distribution, which is similar to Lemma 6.

Next we analyze the dynamics of $p_{\theta(t)}(\mathbf{B}_i | \mathbf{A}_i \rightarrow)$ and $p_{\theta(t)}(\mathbf{A}_i | \mathbf{B}_i \leftarrow)$.

Proposition 4.2 (Next token probability). *For input sequence (x_1, x_2) , the next token probability under parameters $\theta(t)$ is*

$$p_{\theta(t)}(x | x_1, x_2) = \frac{\exp(Y(t)_{x_1, x})}{\sum_{x' \in [M]} \exp(Y(t)_{x_1, x'})},$$

where $Y(t)_{i,j}$ is the entry of the matrix $Y(t)$ at row i and column j .

The proof is also deferred to Appendix B.1.1. According to Proposition 4.2, the next token probability when the entity in the input is x_1 is determined by the x_1 -th row of the matrix $Y(t)$. Another nice property indicated by Proposition 4.2 is that we don't need to keep track of the dynamics of $Z(t)$, which could greatly simplify the analysis. The following lemma shows the dynamics of $Y(t)$.

Lemma 2 (Dynamics of $Y(t)$). Assume we run SGD with batch size 1³, and assume $M \gg 100$ and $\frac{1}{M^{0.99}} \ll \eta_Y < 1$. Let $t \gtrsim \frac{N \ln M}{\eta_Y}$ and let $Y(t)_i$ denote the i -th row of $Y(t)$ and $Y(t)_{ij}$ denote the entry of $Y(t)$ at row i and column j . Then for training sequence $(x_1, x_2, x_3) \in \mathcal{D}_{train}$ at time t , we have

$$Y(t)_{x_1, x_3} \gtrsim \ln \left(\frac{M \eta_Y t}{N} \right), \quad \text{and} \quad Y(t)_{x_1, x} \lesssim -\frac{1}{M} \ln \left(\frac{M \eta_Y t}{N} \right), \quad \forall x \neq x_3.$$

and for any test sequence $(x_1, x_2, x_3) \in \mathcal{D}_{test}$, we have

$$Y(t)_{x_1, x} = 0, \forall x \in [M].$$

The proof of [Lemma 2](#) is presented in [Appendix B.1.2](#). [Lemma 2](#) implies the asymmetry of the model weights $Y(t)$: for two tokens x_1, x_3 , when x_1 appears as a contextual token and x_3 serves as the next token in the same training sequence, the model weights $Y(t)_{x_1, x_3}$ gets increased during training while $Y(t)_{x_3, x_1}$ will not get increased. Combining [Proposition 4.2](#), we can obtain our main theorem for the reversal curse.

Theorem 3 (Reversal curse). Assume we run SGD with batch size 1, and assume $M \gg 100$ and $\frac{1}{M^{0.99}} \ll \eta_Y < 1$. Let $t \gtrsim \frac{N \ln M}{\eta_Y}$ denote the time step which also satisfies $\ln t \gtrsim \ln(NM/\eta_Y)$. For training sequence $(x_1, x_2, x_3) \in \mathcal{D}_{train}$ at time t , we have

$$p_{\theta(t)}(x_3|x_1, x_2) \geq 1 - \frac{M-1}{2 \left(\frac{M \eta_Y t}{N} \right)^c} \xrightarrow{t \rightarrow \infty} 1$$

for some constant $c > 0$, and for any test sequence $(x_1, x_2, x_3) \in \mathcal{D}_{test}$ that is not included the training set \mathcal{D}_{train} , we have

$$p_{\theta(t)}(x_3|x_1, x_2) \leq \frac{1}{M}.$$

[Theorem 3](#) shows that although the direction presented in the training set can be learned nearly perfectly, the model’s next token prediction of the reverse direction is almost a random guess. The proof is deferred to [Appendix B.1.3](#). We also empirically validate the above results for multi-layer transformers in [Section 5.1](#).

4.2 Chain-of-thought

In this section, we extend our analysis in [Section 4.1](#) to study other logical relationships beyond the reversal curse. In particular, we study chain-of-thought (COT) ([Wei et al., 2022b](#)) and show the necessity of COT via training dynamics.

COT encourages LLMs to output a series of intermediate reasoning steps to increase their performance. Consider the simplest example, where the model learns two facts that $A \rightarrow B$ and $B \rightarrow C$, and we want to test whether the model is able to directly conclude that $A \rightsquigarrow C$. COT indicates that if an LLM is only trained on $A \rightarrow B$ and $B \rightarrow C$, it would be easier for the model to deduce $A \rightsquigarrow C$ during the inference time if the model can first output the intermediate steps $A \rightarrow B$ and $B \rightarrow C$, instead of directly predicting the next token C given the input “ $A \rightsquigarrow$ ”. The failure of directly deducing $A \rightsquigarrow C$ is also empirically observed by [Allen-Zhu and Li \(2023\)](#).

Theoretically, [Feng et al. \(2024\)](#) shows the necessity of COT for some complex reasoning tasks through the lens of the expressivity of transformers. In this section, we show the necessity of COT through a different angle, i.e., training dynamics. We show that for the above simplest two-step reasoning, without COT, the model is not able to directly predict C given the input “ $A \rightsquigarrow$ ” even if it learns $A \rightarrow B$ and $B \rightarrow C$.

³The lemma holds even if the batch size is larger than 1 and the analysis is essentially the same.

Datasets. Let $N_{\text{train}} > 0$, $N_{\text{test}} > 0$ be two positive integers and let $N_{\text{total}} = N_{\text{train}} + N_{\text{test}}$. Let $\mathbf{A}_i, \mathbf{B}_i, \mathbf{C}_i \in \mathcal{V}, \forall i \in [N_{\text{total}}]$ be $3N_{\text{total}}$ distinct tokens. Let $\rightarrow, \rightsquigarrow \in \mathcal{V} = [M]$ be two additional different tokens that represent “direct implication” and “indirect implication” respectively. Specifically, we have $\mathbf{A}_i \rightarrow \mathbf{B}_i$, $\mathbf{B}_i \rightarrow \mathbf{C}_i$ and $\mathbf{A}_i \rightsquigarrow \mathbf{C}_i$ for all $i \in [N_{\text{total}}]$. For notation convenience, we define the following two index sets

$$\mathcal{I}_{\text{train}} = \{1, 2, \dots, N_{\text{train}}\}, \quad \mathcal{I}_{\text{test}} = \{N_{\text{train}} + 1, \dots, N_{\text{total}}\}.$$

The training set $\mathcal{D}_{\text{train}}$ consists of all $\mathbf{A}_i \rightarrow \mathbf{B}_i$, $\mathbf{B}_i \rightarrow \mathbf{C}_i$ and $\mathbf{A}_i \rightsquigarrow \mathbf{C}_i$ for $i \in \mathcal{I}_{\text{train}}$. In addition, $\mathcal{D}_{\text{train}}$ contains $\mathbf{A}_i \rightarrow \mathbf{B}_i$ and $\mathbf{B}_i \rightarrow \mathbf{C}_i$ for $i \in \mathcal{I}_{\text{test}}$. For convenience, we let $N = |\mathcal{D}_{\text{train}}|$ to be the size of the training set. The test set $\mathcal{D}_{\text{test}}$ consists of $\mathbf{A}_i \rightsquigarrow \mathbf{C}_i$ for $i \in \mathcal{I}_{\text{test}}$. Under our construction of the dataset, the LLM will learn the relationship between \mathbf{A}_i , \mathbf{B}_i and \mathbf{C}_i for $i \in \mathcal{I}_{\text{train}}$ in both direct and indirect implication, and learn the relationship between \mathbf{A}_i , \mathbf{B}_i and \mathbf{C}_i for $i \in \mathcal{I}_{\text{test}}$ only in direct implication and will be tested for indirect implication.

Similar to the reversal curse in [Section 4.1](#), we aim to prove through the training dynamics of one-layer transformers that the test probability remains negligible during training. In particular, we are interested in

$$p_{\theta}(x_3 = \mathbf{C}_i | x_1 = \mathbf{A}_i, x_2 = \rightsquigarrow), \quad i \in \mathcal{I}_{\text{test}}.$$

We also use $p_{\theta}(\mathbf{B}_i | \mathbf{A}_i \rightarrow)$, $p_{\theta}(\mathbf{C}_i | \mathbf{B}_i \rightarrow)$ and $p_{\theta}(\mathbf{C}_i | \mathbf{A}_i \rightsquigarrow)$ to more compactly represent $p_{\theta}(x_3 = \mathbf{B}_i | x_1 = \mathbf{A}_i, x_2 = \rightarrow)$, $p_{\theta}(x_3 = \mathbf{C}_i | x_1 = \mathbf{B}_i, x_2 = \rightarrow)$ and $p_{\theta}(x_3 = \mathbf{C}_i | x_1 = \mathbf{A}_i, x_2 = \rightsquigarrow)$, respectively.

The following theorem shows the necessity of the chain-of-thought method:

Theorem 4 (Necessity of chain-of-thought). *Assume we run SGD with batch size 1, and assume $M \gg 100$ and $\frac{1}{M^{0.99}} \ll \eta_Y < 1$. Let $t \gtrsim \frac{N \ln M}{\eta_Y}$ denote the time step which also satisfies $\ln t \gtrsim \ln(NM/\eta_Y)$. For any test index $i \in \mathcal{I}_{\text{test}}$, we have*

$$p_{\theta(t)}(\mathbf{B}_i | \mathbf{A}_i \rightarrow) \geq 1 - \frac{M-1}{2 \left(\frac{M\eta_Y t}{N} \right)^c}, \quad p_{\theta(t)}(\mathbf{C}_i | \mathbf{B}_i \rightarrow) \geq 1 - \frac{M-1}{2 \left(\frac{M\eta_Y t}{N} \right)^c}$$

for some constant $c > 0$ and

$$p_{\theta(t)}(\mathbf{C}_i | \mathbf{A}_i \rightsquigarrow) \leq \frac{1}{M}.$$

We defer the proof to [Appendix B.2](#). [Theorem 4](#) shows that although the LLM learns $\mathbf{A}_i \rightarrow \mathbf{B}_i$ and $\mathbf{B}_i \rightarrow \mathbf{C}_i$ nearly perfectly, it cannot directly deduce $\mathbf{A}_i \rightsquigarrow \mathbf{C}_i$. Analogous to the asymmetry of causal transformer weights as we discussed in [Section 4.1](#), our analysis of COT reveals another property, i.e., intransitivity: training the weights associated with **A** to **B** and **B** to **C** does not necessarily increase the weights associated with **A** to **C**.

4.3 Roles of the attention score matrix

During the analysis of [Sections 4.1](#) and [4.2](#), we show that the reversal curse and the necessity of COT are largely due to the asymmetry and intransitivity of causal transformer weights (in our case, the weight matrix $Y(t)$). However, it seems that the dynamics of the attention score matrix $Z(t)$ do not impact the model performance. Below, we briefly discuss the role of the attention score matrix $Z(t)$.

In [\(7\)](#), the attention score is used to calculate the weights b_{tT} , where a contextual token x_t with a larger attention score attended by the query token x_T has a larger weight. Note that we use the

same formulation as the previous work [Tian et al. \(2023a\)](#) where the query token will not attend to itself. Therefore, for a three-token training sequence, the weights b_{12} is always one since there is only one contextual token x_1 , no matter whether the value of the attention score is high or low.

However, consider a slightly different setting, where the relationship is represented by two tokens. In that case, $x_1 = A_i, x_2 = R_1, x_3 = R_2, x_4 = B_i$, and there are two contextual tokens $x_1 = A_i$ and $x_2 = R_1$. The role of the attention score in this case is to select the important token, i.e., A_i , by putting more weight on it. Theorem 2 of [Tian et al. \(2023a\)](#) showed that under certain technical assumptions, the query token R_2 will attend more to “distinct tokens” A_i and less to the “common token” R_1 . Therefore, the query token R_2 will eventually put all weights to A_i , and the remaining analysis remains the same as in [Sections 4.1](#) and [4.2](#).

5 Experiments

In this section, we conduct experiments to further validate our theoretical results in [Section 4](#) on multi-layer transformers. We show experimental results of the reversal curse and chain-of-thought in [Section 5.1](#), [Section 5.2](#), respectively.

5.1 Reversal Curse

In [Section 3](#) and [Section 4](#), we theoretically proved the reversal curse for both the bilinear model and one-layer transformer under certain assumptions. Now, we empirically show that the reversal curse still happens even for multi-layer transformers.

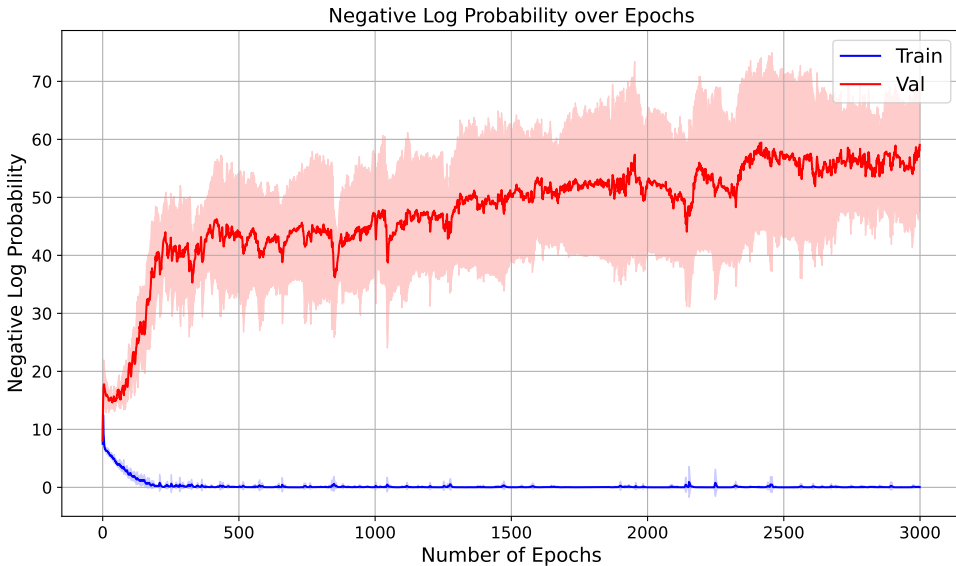


Figure 1: Experiment results of reversal curse under default configuration (see [Table 3](#)). The curves represent the (average) negative log probability of the model predicting the next token to be B_i when the input is “ $A_i \rightarrow$ ”, or to be A_i when the input is “ $B_i \leftarrow$ ”. While the sentences in the training set can be learned nearly perfectly (as shown by the training curve where the next token probability converges to one), the model is not able to predict the correct next token in the validation set better than a uniformly random guess. Both curves are averaged over 10 random seeds.

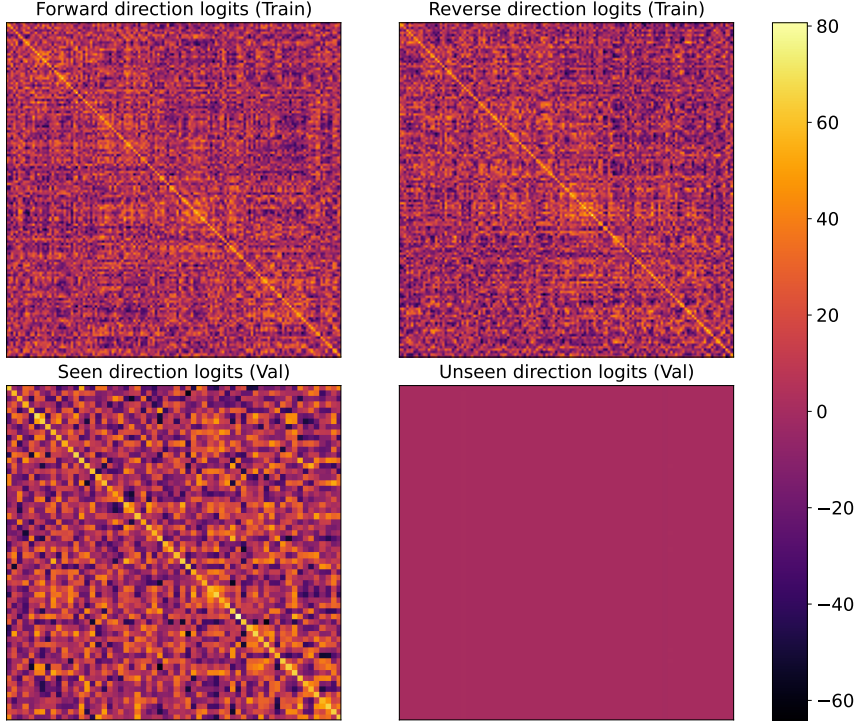


Figure 2: Visualization of the weights (logits) of the model with default configurations trained after 3000 epochs for the reversal curse experiment. For the top-left matrix, the i -th row corresponds to an entity token A_i for a training pair, and the i -th column corresponds to an entity token B_i for a training pair. The (i, j) -th entry represents the model weights from the token A_i to B_j , i.e., the logits of B_j when the input sequence consists of only A_i . Similarly, for the bottom-left matrix, the row corresponds to the input entity tokens of the seen direction (the direction included in the training set) of validation pairs, and the column corresponds to output entity tokens. The two matrices on the right are obtained by swapping row tokens and column tokens of their corresponding left matrices. Note that the diagonals of the bottom-right matrix are all close to zero, while the diagonals of other matrices all have large values. This implies that if a pair of tokens (A, B) only appear in the training set in one direction, then the model weights associated with the other direction will hardly get trained.

Dataset construction. Below, we describe how we generate our synthetic dataset for experiments on the reversal curse. We choose the vocabulary $\mathcal{V} = \{0, 1, \dots, N\}$ for a specified $N > 0$. We randomly sample two disjoint sets of entities $\mathcal{A}, \mathcal{B} \subset \mathcal{V}$ with $|\mathcal{A}| = |\mathcal{B}| = |\mathcal{V}|/4$, and reserve two additional tokens for relationships \rightarrow and \leftarrow , respectively.⁴ Next, we specify a bijection from \mathcal{A} to \mathcal{B} uniformly at random. For each $A_i \in \mathcal{A}$ and its corresponding $B_i \in \mathcal{B}$, we can obtain a pair of sequence $(A_i \rightarrow B_i, B_i \leftarrow A_i)$. We split the set of all pairs into training pairs and validation pairs. For each training pair, both sequences will be included in the training set, while for the validation pair, we randomly select one sequence for the training set and the other for the validation set. Therefore, the model will learn both directions for the training pairs and only one direction for each validation pair while being tested in the unseen direction.

⁴By default, each entity is represented by a single token in \mathcal{V} . See additional experiments in multi-token settings in [Appendices C.2](#) and [C.3](#)

Model architectures. We train multi-layer transformers based on GPT-2 architecture. [Figure 1](#) shows the results where the model has 24 layers, 12 attention heads per layer, uses absolute positional encoding, and we choose the vocabulary size of 800. The training set size is 340, and the validation set size is 60 (resulting from 140 training pairs and 60 validation pairs). We also conducted experiments with various model configurations and vocabulary sizes in [Appendix C.2](#). Besides, all hyperparameters and different model configurations are presented in [Appendix C.1](#).

Results. [Figure 1](#) shows that during the training, the next token probability for training data increases a lot while the next token probability for validation data remains unchanged or gets even smaller. This is consistent with our theoretical results of [Theorem 3](#).

According to our theoretical analysis, the reversal curse happens due to the asymmetry of model (re-parameterized) weights (i.e., logits of a token given another token as input), and we also empirically validate the asymmetry for multi-layer transformers. [Figure 2](#) shows the model weights from a token x_1 to x_3 is trained large for a training sequence (x_1, x_2, x_3) as represented by the diagonals of the first three matrices, while the weights from a token x_1 to x_3 remains nearly zero for a validation sequence (x_1, x_2, x_3) as represented by the diagonals of the last matrix, which is consistent with [Lemma 2](#). This implies that if a pair of tokens (A, B) only appear in the training set in one direction, then the model weights associated with the other direction will hardly get trained.

5.2 Chain-of-thought

We also conduct experiments for COT on multi-layer transformers to validate results in [Section 4.2](#).

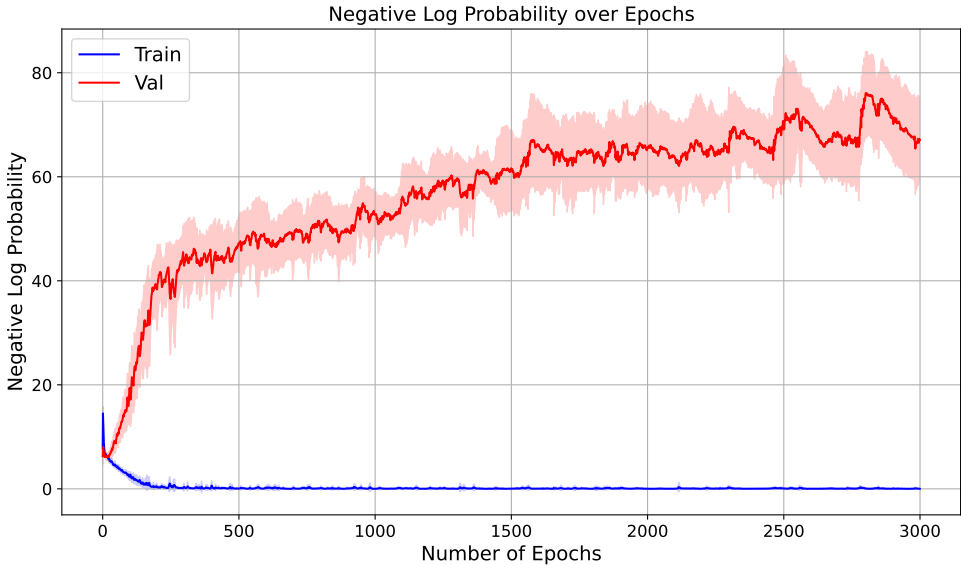


Figure 3: Experiment results of COT under default configuration (see [Table 3](#)). The curves represent the (average) negative log probability of the model predicting the next token to be: (1) B_i given the input “ $A_i \rightarrow$ ”, (2) C_i given the input “ $B_i \rightarrow$ ”, or (3) C_i given the input “ $A_i \rightsquigarrow$ ”. Similar to the reversal curse experiment, while the sentences in the training set can be learned nearly perfectly, the model is not able to predict the correct next token in the validation set better than a uniformly random guess. Both curves are averaged over 10 random seeds.

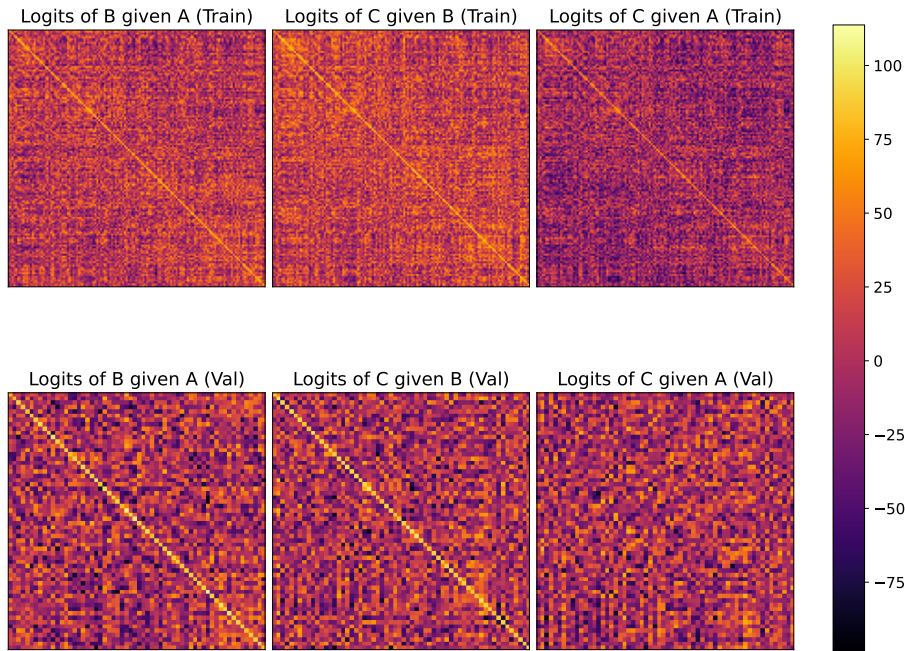


Figure 4: Visualization of the weights (logits) of the model with default configurations trained after 3000 epochs for COT experiment. The matrices are similar to Figure 2. The row tokens for the top matrices are A_i, B_i, A_i and column tokens are B_i, C_i, C_i for training triples respectively. Similarly, the bottom matrices correspond to validation triples. For validation triples (A_i, B_i, C_i) , the weights from A_i to C_i get hardly trained as indicated by the diagonals of the last matrix.

Dataset construction. Similar to Section 5.1, we randomly sample three disjoint sets of entities $\mathcal{A}, \mathcal{B}, \mathcal{C} \subset \mathcal{V}$, and reverse two additional tokens for \rightarrow and \rightsquigarrow , respectively. Next, we specify a bijection from \mathcal{A} to \mathcal{B} , and a bijection from \mathcal{B} to \mathcal{C} randomly. For each $A_i \in \mathcal{A}$ and its corresponding $B_i \in \mathcal{B}$ and $C_i \in \mathcal{C}$, we can obtain a triple of sequences $(A_i \rightarrow B_i, B_i \rightarrow C_i, A_i \rightsquigarrow C_i)$, and split the set of all triples into training triples and validation triples. All three sequences of a training triple will be added to the training set, while for a validation triple, we add $A_i \rightarrow B_i$ and $B_i \rightarrow C_i$ to the training set and add $A_i \rightsquigarrow C_i$ to the validation set. Therefore, the model will learn both direct and indirect implications for the training triples and only learn the direct implications for each validation triple while being tested on the indirect implication.

Results. Figure 3 shows the experiment results for COT using the same model architecture and configurations as in Figure 1 (the training set size is 540, and the validation set size is 60 resulting from 140 training triples and 60 validation triples), which is consistent with Theorem 4. One can refer to Appendix C.3 for additional experiments with various model configurations and vocabulary sizes. We also empirically validate the intransitivity of model weights (i.e., logits) for multi-layer transformers in Figure 4, which shows that for a validation triple (A_i, B_i, C_i) of which only the direct implication “ $A_i \rightarrow B_i$ ” and “ $B_i \rightarrow C_i$ ” appears in the training set, although the weights from A_i to B_i and from B_i to C_i are trained large as indicated by the diagonals of the first two bottom matrices, the weights from A_i to C_i gets hardly trained as indicated by the diagonals of the last matrix. We also emphasize that another reason that COT is necessary is that all tokens A_i, B_i , and C_i are different

tokens with randomly initialized embedding and thus irrelevant. When these tokens are relevant and show specific patterns, the validation loss can also get better. See more details in [Appendix C.4](#).

6 Conclusions

In this paper, we study the reversal curse theoretically via training dynamics of (1) a bilinear model, which is a simplification of the one-layer transformer; (2) one-layer transformers under certain technical assumptions similar to [Tian et al. \(2023a\)](#). Our theoretical results suggest that a core reason the reversal curse happens in auto-regressive LLMs is the asymmetry of the model weights, and we apply the same technique to prove the necessity of COT for one-layer transformers, which is mainly due to the intransitivity of model weights. The asymmetry and intransitivity of model weights indicate that an auto-regressive LLM might mainly focus on learning text sequences during training *separately* instead of automatically deducing indirect conclusions due to the next token prediction objective and causal transformer-based structures. This highlights the importance of ICL, data augmentation, or planning for current auto-regressive LLMs to solve complex reasoning tasks.

As for future directions, it would be interesting and important to study: (1) What is a unified way to characterize and study the reversal curse, COT, and other similar logical reasoning tasks? (2) Our paper mainly focuses on three-token sequences, where each entity or relationship is represented by a single token. While we empirically explored the setting where each entity might consist of multiple tokens and distinct entities might share a few tokens, it would be interesting to analyze the multiple-token setting theoretically. (3) We theoretically analyzed the bilinear model and one-layer transformer, and it would be an important future direction to extend the analysis to multi-layer transformers.

References

- Ekin Akyürek, Dale Schuurmans, Jacob Andreas, Tengyu Ma, and Denny Zhou. What learning algorithm is in-context learning? investigations with linear models. *arXiv preprint arXiv:2211.15661*, 2022.
- Zeyuan Allen-Zhu and Yuanzhi Li. Physics of language models: Part 3.2, knowledge manipulation. *arXiv preprint arXiv:2309.14402*, 2023.
- Cem Anil, Yuhuai Wu, Anders Andreassen, Aitor Lewkowycz, Vedant Misra, Vinay Ramasesh, Ambrose Slone, Guy Gur-Ari, Ethan Dyer, and Behnam Neyshabur. Exploring length generalization in large language models. *arXiv preprint arXiv:2207.04901*, 2022.
- Yu Bai, Fan Chen, Huan Wang, Caiming Xiong, and Song Mei. Transformers as statisticians: Provable in-context learning with in-context algorithm selection. *arXiv preprint arXiv:2306.04637*, 2023.
- Boaz Barak, Benjamin Edelman, Surbhi Goel, Sham Kakade, Eran Malach, and Cyril Zhang. Hidden progress in deep learning: Sgd learns parities near the computational limit. *Advances in Neural Information Processing Systems*, 35:21750–21764, 2022.
- Lukas Berglund, Meg Tong, Max Kaufmann, Mikita Balesni, Asa Cooper Stickland, Tomasz Korbak, and Owain Evans. The reversal curse: Llms trained on "a is b" fail to learn "b is a". *arXiv preprint arXiv:2309.12288*, 2023.

- Satwik Bhattamishra, Kabir Ahuja, and Navin Goyal. On the ability and limitations of transformers to recognize formal languages. *arXiv preprint arXiv:2009.11264*, 2020a.
- Satwik Bhattamishra, Arkil Patel, and Navin Goyal. On the computational power of transformers and its implications in sequence modeling. *arXiv preprint arXiv:2006.09286*, 2020b.
- Alberto Bietti, Vivien Cabannes, Diane Bouchacourt, Herve Jegou, and Leon Bottou. Birth of a transformer: A memory viewpoint. *arXiv preprint arXiv:2306.00802*, 2023.
- Enric Boix-Adsera, Etai Littwin, Emmanuel Abbe, Samy Bengio, and Joshua Susskind. Transformers learn through gradual rank increase. *arXiv preprint arXiv:2306.07042*, 2023.
- Jannik Brinkmann, Abhay Sheshadri, Victor Levoso, Paul Swoboda, and Christian Bartelt. A mechanistic analysis of a transformer trained on a symbolic multi-step reasoning task. *arXiv preprint arXiv:2402.11917*, 2024.
- Tom Brown, Benjamin Mann, Nick Ryder, Melanie Subbiah, Jared D Kaplan, Prafulla Dhariwal, Arvind Neelakantan, Pranav Shyam, Girish Sastry, Amanda Askell, et al. Language models are few-shot learners. *Advances in neural information processing systems*, 33:1877–1901, 2020.
- Yupeng Chang, Xu Wang, Jindong Wang, Yuan Wu, Linyi Yang, Kaijie Zhu, Hao Chen, Xiaoyuan Yi, Cunxiang Wang, Yidong Wang, et al. A survey on evaluation of large language models. *ACM Transactions on Intelligent Systems and Technology*, 2023.
- Karl Cobbe, Vineet Kosaraju, Mohammad Bavarian, Mark Chen, Heewoo Jun, Lukasz Kaiser, Matthias Plappert, Jerry Tworek, Jacob Hilton, Reiichiro Nakano, et al. Training verifiers to solve math word problems. *arXiv preprint arXiv:2110.14168*, 2021.
- Mostafa Dehghani, Stephan Gouws, Oriol Vinyals, Jakob Uszkoreit, and Łukasz Kaiser. Universal transformers. *arXiv preprint arXiv:1807.03819*, 2018.
- Benjamin L Edelman, Surbhi Goel, Sham Kakade, and Cyril Zhang. Inductive biases and variable creation in self-attention mechanisms. In *International Conference on Machine Learning*, pages 5793–5831. PMLR, 2022.
- Nelson Elhage, Neel Nanda, Catherine Olsson, Tom Henighan, Nicholas Joseph, Ben Mann, Amanda Askell, Yuntao Bai, Anna Chen, Tom Conerly, et al. A mathematical framework for transformer circuits. *Transformer Circuits Thread*, 1:1, 2021.
- Guhao Feng, Bohang Zhang, Yuntian Gu, Haotian Ye, Di He, and Liwei Wang. Towards revealing the mystery behind chain of thought: a theoretical perspective. *Advances in Neural Information Processing Systems*, 36, 2024.
- Hengyu Fu, Tianyu Guo, Yu Bai, and Song Mei. What can a single attention layer learn? a study through the random features lens. *Advances in Neural Information Processing Systems*, 36, 2024.
- Shivam Garg, Dimitris Tsipras, Percy S Liang, and Gregory Valiant. What can transformers learn in-context? a case study of simple function classes. *Advances in Neural Information Processing Systems*, 35:30583–30598, 2022.
- Olga Golovneva, Zeyuan Allen-Zhu, Jason Weston, and Sainbayar Sukhbaatar. Reverse training to nurse the reversal curse. *arXiv preprint arXiv:2403.13799*, 2024.

- Qingyan Guo, Rui Wang, Junliang Guo, Xu Tan, Jiang Bian, and Yujiu Yang. Mitigating reversal curse via semantic-aware permutation training. *arXiv preprint arXiv:2403.00758*, 2024.
- Simon Jerome Han, Keith J Ransom, Andrew Perfors, and Charles Kemp. Inductive reasoning in humans and large language models. *Cognitive Systems Research*, 83:101155, 2024.
- Jiri Hron, Yasaman Bahri, Jascha Sohl-Dickstein, and Roman Novak. Infinite attention: Nngp and ntk for deep attention networks. In *International Conference on Machine Learning*, pages 4376–4386. PMLR, 2020.
- Wenlong Huang, Pieter Abbeel, Deepak Pathak, and Igor Mordatch. Language models as zero-shot planners: Extracting actionable knowledge for embodied agents. In *International Conference on Machine Learning*, pages 9118–9147. PMLR, 2022.
- Yu Huang, Yuan Cheng, and Yingbin Liang. In-context convergence of transformers. *arXiv preprint arXiv:2310.05249*, 2023.
- Samy Jelassi, Michael Sander, and Yuanzhi Li. Vision transformers provably learn spatial structure. *Advances in Neural Information Processing Systems*, 35:37822–37836, 2022.
- Jaehun Jung, Lianhui Qin, Sean Welleck, Faeze Brahman, Chandra Bhagavatula, Ronan Le Bras, and Yejin Choi. Maieutic prompting: Logically consistent reasoning with recursive explanations. *arXiv preprint arXiv:2205.11822*, 2022.
- Takeshi Kojima, Shixiang Shane Gu, Machel Reid, Yutaka Matsuo, and Yusuke Iwasawa. Large language models are zero-shot reasoners. *Advances in neural information processing systems*, 35: 22199–22213, 2022.
- Beatrice Laurent and Pascal Massart. Adaptive estimation of a quadratic functional by model selection. *Annals of Statistics*, pages 1302–1338, 2000.
- Shuai Li, Zhao Song, Yu Xia, Tong Yu, and Tianyi Zhou. The closeness of in-context learning and weight shifting for softmax regression. *arXiv preprint arXiv:2304.13276*, 2023.
- Valerii Likhoshesterov, Krzysztof Choromanski, and Adrian Weller. On the expressive power of self-attention matrices. *arXiv preprint arXiv:2106.03764*, 2021.
- Licong Lin, Yu Bai, and Song Mei. Transformers as decision makers: Provable in-context reinforcement learning via supervised pretraining. *arXiv preprint arXiv:2310.08566*, 2023.
- Bingbin Liu, Jordan T Ash, Surbhi Goel, Akshay Krishnamurthy, and Cyril Zhang. Transformers learn shortcuts to automata. *arXiv preprint arXiv:2210.10749*, 2022.
- Ilya Loshchilov and Frank Hutter. Decoupled weight decay regularization. *arXiv preprint arXiv:1711.05101*, 2017.
- Ruilin Luo, Tianle Gu, Haoling Li, Junzhe Li, Zicheng Lin, Jiayi Li, and Yujiu Yang. Chain of history: Learning and forecasting with llms for temporal knowledge graph completion. *arXiv preprint arXiv:2401.06072*, 2024.
- Ang Lv, Kaiyi Zhang, Shufang Xie, Quan Tu, Yuhan Chen, Ji-Rong Wen, and Rui Yan. Are we falling in a middle-intelligence trap? an analysis and mitigation of the reversal curse. *arXiv preprint arXiv:2311.07468*, 2023.

- Arvind Mahankali, Tatsunori B Hashimoto, and Tengyu Ma. One step of gradient descent is provably the optimal in-context learner with one layer of linear self-attention. *arXiv preprint arXiv:2307.03576*, 2023.
- Song Mei and Yuchen Wu. Deep networks as denoising algorithms: Sample-efficient learning of diffusion models in high-dimensional graphical models. *arXiv preprint arXiv:2309.11420*, 2023.
- Eshaan Nichani, Alex Damian, and Jason D Lee. How transformers learn causal structure with gradient descent. *arXiv preprint arXiv:2402.14735*, 2024.
- Maxwell Nye, Anders Johan Andreassen, Guy Gur-Ari, Henryk Michalewski, Jacob Austin, David Bieber, David Dohan, Aitor Lewkowycz, Maarten Bosma, David Luan, et al. Show your work: Scratchpads for intermediate computation with language models. *arXiv preprint arXiv:2112.00114*, 2021.
- Catherine Olsson, Nelson Elhage, Neel Nanda, Nicholas Joseph, Nova DasSarma, Tom Henighan, Ben Mann, Amanda Askell, Yuntao Bai, Anna Chen, et al. In-context learning and induction heads. *arXiv preprint arXiv:2209.11895*, 2022.
- Jorge Pérez, Pablo Barceló, and Javier Marinkovic. Attention is turing-complete. *Journal of Machine Learning Research*, 22(75):1–35, 2021.
- Chengwen Qi, Bowen Li, Binyuan Hui, Bailin Wang, Jinyang Li, Jinwang Wu, and Yuanjun Laili. An investigation of llms’ inefficacy in understanding converse relations. *arXiv preprint arXiv:2310.05163*, 2023.
- Laria Reynolds and Kyle McDonell. Prompt programming for large language models: Beyond the few-shot paradigm. In *Extended Abstracts of the 2021 CHI Conference on Human Factors in Computing Systems*, pages 1–7, 2021.
- Charlie Snell, Ruiqi Zhong, Dan Klein, and Jacob Steinhardt. Approximating how single head attention learns. *arXiv preprint arXiv:2103.07601*, 2021.
- Jianlin Su, Murtadha Ahmed, Yu Lu, Shengfeng Pan, Wen Bo, and Yunfeng Liu. Roformer: Enhanced transformer with rotary position embedding. *Neurocomputing*, 568:127063, 2024.
- Yuandong Tian, Yiping Wang, Beidi Chen, and Simon Du. Scan and snap: Understanding training dynamics and token composition in 1-layer transformer, 2023a.
- Yuandong Tian, Yiping Wang, Zhenyu Zhang, Beidi Chen, and Simon Du. Joma: Demystifying multilayer transformers via joint dynamics of mlp and attention. *arXiv preprint arXiv:2310.00535*, 2023b.
- Karthik Valmeekam, Alberto Olmo, Sarath Sreedharan, and Subbarao Kambhampati. Large language models still can’t plan (a benchmark for llms on planning and reasoning about change). *arXiv preprint arXiv:2206.10498*, 2022.
- Ashish Vaswani, Noam Shazeer, Niki Parmar, Jakob Uszkoreit, Llion Jones, Aidan N Gomez, Łukasz Kaiser, and Illia Polosukhin. Attention is all you need. *Advances in neural information processing systems*, 30, 2017.
- Johannes Von Oswald, Eyvind Niklasson, Ettore Randazzo, João Sacramento, Alexander Mordvintsev, Andrey Zhmoginov, and Max Vladymyrov. Transformers learn in-context by gradient descent. *arXiv preprint arXiv:2212.07677*, 2022.

- Johannes Von Oswald, Eyvind Niklasson, Ettore Randazzo, João Sacramento, Alexander Mordvintsev, Andrey Zhmoginov, and Max Vladymyrov. Transformers learn in-context by gradient descent. In *International Conference on Machine Learning*, pages 35151–35174. PMLR, 2023.
- Xuezhi Wang, Jason Wei, Dale Schuurmans, Quoc Le, Ed Chi, Sharan Narang, Aakanksha Chowdhery, and Denny Zhou. Self-consistency improves chain of thought reasoning in language models. *arXiv preprint arXiv:2203.11171*, 2022.
- Colin Wei, Yining Chen, and Tengyu Ma. Statistically meaningful approximation: a case study on approximating turing machines with transformers. *Advances in Neural Information Processing Systems*, 35:12071–12083, 2022a.
- Jason Wei, Xuezhi Wang, Dale Schuurmans, Maarten Bosma, Fei Xia, Ed Chi, Quoc V Le, Denny Zhou, et al. Chain-of-thought prompting elicits reasoning in large language models. *Advances in neural information processing systems*, 35:24824–24837, 2022b.
- Sang Michael Xie, Aditi Raghunathan, Percy Liang, and Tengyu Ma. An explanation of in-context learning as implicit bayesian inference. *arXiv preprint arXiv:2111.02080*, 2021.
- Greg Yang, Edward J Hu, Igor Babuschkin, Szymon Sidor, Xiaodong Liu, David Farhi, Nick Ryder, Jakub Pachocki, Weizhu Chen, and Jianfeng Gao. Tensor programs v: Tuning large neural networks via zero-shot hyperparameter transfer. *arXiv preprint arXiv:2203.03466*, 2022.
- Shunyu Yao, Binghui Peng, Christos Papadimitriou, and Karthik Narasimhan. Self-attention networks can process bounded hierarchical languages. *arXiv preprint arXiv:2105.11115*, 2021.
- Chulhee Yun, Srinadh Bhojanapalli, Ankit Singh Rawat, Sashank J Reddi, and Sanjiv Kumar. Are transformers universal approximators of sequence-to-sequence functions? *arXiv preprint arXiv:1912.10077*, 2019.
- Eric Zelikman, Yuhuai Wu, Jesse Mu, and Noah Goodman. Star: Bootstrapping reasoning with reasoning. *Advances in Neural Information Processing Systems*, 35:15476–15488, 2022.
- Dylan Zhang, Curt Tigges, Zory Zhang, Stella Biderman, Maxim Raginsky, and Talia Ringer. Transformer-based models are not yet perfect at learning to emulate structural recursion. *arXiv preprint arXiv:2401.12947*, 2024.
- Jingzhao Zhang, Tianxing He, Suvrit Sra, and Ali Jadbabaie. Why gradient clipping accelerates training: A theoretical justification for adaptivity. In *International Conference on Learning Representations*, 2020.
- Ruiqi Zhang, Spencer Frei, and Peter L Bartlett. Trained transformers learn linear models in-context. *arXiv preprint arXiv:2306.09927*, 2023.
- Haoyu Zhao, Abhishek Panigrahi, Rong Ge, and Sanjeev Arora. Do transformers parse while predicting the masked word? *arXiv preprint arXiv:2303.08117*, 2023.

A Missing Proofs of Section 3

Theorem 5 (Separation of training dynamics, formal statement of [Theorem 1](#)). *Fix arbitrary $\delta, \epsilon \in (0, 1)$. Let v_1, \dots, v_m be independently sampled from $\mathcal{N}_d(\mathbf{0}_d, \frac{1}{d}I_d)$. Let x_1, \dots, x_n and y_1, \dots, y_n be sampled uniformly at random from $\{v_1, \dots, v_m\}$ without replacement. Define*

$$\begin{aligned}\mathcal{L}(\Theta) &= \frac{1}{2n-1} \left(\sum_{i=1}^n -\log p_{\Theta}(y_i|x_i) + \sum_{i=2}^n -\log p_{\Theta}(x_i|y_i) \right) \\ \mathcal{L}^{\text{rev}}(\Theta) &= -\log p_{\Theta}(x_1|y_1).\end{aligned}$$

Consider the gradient flow $\Theta_t : t \geq 0$ where $\Theta_0 \sim \mathcal{N}(\mathbf{0}^{\otimes 2}, \sigma^2 \cdot I^{\otimes 2})$ and

$$\frac{d\Theta_t}{dt} = -\nabla \mathcal{L}(\Theta_t).$$

Suppose $\sigma \leq \frac{1}{100 \ln(64m^2/\delta)}$ and

$$d \geq \frac{10^6 n^4 m^2 \log^4(2m) \log(64m^2 n^2/\delta)}{\epsilon^2}$$

With probability at least $1 - \delta$, we have

$$\frac{\mathcal{L}^{\text{rev}}(\Theta_t)}{\mathcal{L}^{\text{rev}}(\Theta_0)} \geq \left(\frac{\mathcal{L}(\Theta_t)}{\mathcal{L}(\Theta_0)} \right)^{\epsilon}, \quad \forall t \geq 0.$$

Proof. Let $v = \sqrt{\frac{400n^2 m^2 \log(64m^2 n^2/\delta)}{d}}$. By [Lemma 3](#) and [Lemma 4](#), with probability at least $1 - \delta$,

$$\begin{aligned}\mathcal{L}^{\text{rev}}(\Theta_t) &\geq \mathcal{L}^{\text{rev}}(\Theta_0) \cdot \left(1 + \frac{\mathcal{L}(\Theta_0) \cdot t}{8(2n-1) \log^2(2m)} \right)^{-8v(2n-1) \log^2(2m)} \\ &\geq \mathcal{L}^{\text{rev}}(\Theta_0) \cdot \left(\frac{\mathcal{L}(\Theta_t)}{\mathcal{L}(\Theta_0)} \right)^{8v(2n-1) \log^2(2m)}\end{aligned}$$

By definition of d , we have $8v(2n-1) \log^2(2m) \leq \epsilon$. Notice that $\frac{\mathcal{L}(\Theta_t)}{\mathcal{L}(\Theta_0)} < 1$, thus

$$\mathcal{L}^{\text{rev}}(\Theta_t) \geq \mathcal{L}^{\text{rev}}(\Theta_0) \cdot \left(\frac{\mathcal{L}(\Theta_t)}{\mathcal{L}(\Theta_0)} \right)^{\epsilon}.$$

□

Theorem 6 (Lower bound of reversal loss, formal statement of [Theorem 2](#)). *Fix arbitrary $c > 0$ and $C \leq \log(m/2)$. Under the setting of [Theorem 5](#), suppose $\sigma \leq \frac{1}{100 \ln(64m^2/\delta)}$ and*

$$d \geq 10^6 n^4 m^2 \log^4(2m) \log(64m^2 n^2/\delta) \cdot \frac{\log^2 \frac{c}{\log(2m)}}{\log^2 \frac{C}{\log(m/2)}}$$

With probability at least $1 - \delta$,

$$\mathcal{L}^{\text{rev}}(\Theta_{\tau}) \geq C.$$

where τ denotes the first time such that $\mathcal{L}(\Theta_t) \leq c$.

Proof. By continuity, $\mathcal{L}(\Theta_\tau) = c$. By [Theorem 5](#), when

$$d \geq \frac{10^6 n^4 m^2 \log^4(2m) \log(64m^2 n^2 / \delta)}{\epsilon^2} \quad (11)$$

with probability at least $1 - \delta$,

$$\begin{aligned} \mathcal{L}^{\text{rev}}(\Theta_\tau) &\geq \mathcal{L}^{\text{rev}}(\Theta_0) \cdot \left(\frac{\mathcal{L}(\Theta_\tau)}{\mathcal{L}(\Theta_0)} \right)^\epsilon \\ &\geq \mathcal{L}^{\text{rev}}(\Theta_0) \cdot \left(\frac{c}{\mathcal{L}(\Theta_0)} \right)^\epsilon. \end{aligned}$$

Under this event, applying [Lemma 6](#), we can obtain

$$\mathcal{L}^{\text{rev}}(\Theta_\tau) \geq \log(m/2) \cdot \left(\frac{c}{\log(2m)} \right)^\epsilon.$$

To ensure that the right hand side is C , we set $\epsilon = \frac{\log \frac{C}{\log(m/2)}}{\log \frac{c}{\log(2m)}}$. One may check that the definition of d satisfies Eq. (11). It follows that

$$\mathcal{L}^{\text{rev}}(\Theta_\tau) \geq C.$$

□

A.1 Training dynamics

Lemma 3 (Dynamics of the forward loss). *Let $x_1, \dots, x_n, y_1, \dots, y_n, \mathcal{L}(\Theta)$, and Θ_t ($t \geq 0$) be defined as in [Theorem 5](#). When $\sigma \leq \frac{1}{100 \ln(16n^2/\delta)}$ and $d \geq 1600n^3 m^2 \log(8m^2 n^2 / \delta)$, with probability at least $1 - \delta$, we have*

$$\mathcal{L}(\Theta_t) \leq \frac{1}{\frac{t}{8(2n-1)\log^2(2m)} + \frac{1}{\mathcal{L}(\Theta_0)}}, \quad \forall t \geq 0.$$

Furthermore,

$$\inf \{p_{\Theta_t}(x_i|y_i), p_{\Theta_t}(y_i|x_i) : t \geq 0, i \in [n]\} > \frac{1}{2m}.$$

Proof. For convenience, we assume $x_1, \dots, x_n = v_1, \dots, v_n$ and $y_1, \dots, y_n = v_{n+1}, \dots, v_{2n}$ WLOG.

Let $\epsilon = \sqrt{\frac{400n^2 m^2 \log(8m^2 n^2 / \delta)}{d}}$. Then $\epsilon \leq \frac{1}{2\sqrt{n}}$. Define $l_i(\Theta) = -\log p_{\Theta}(y_i|x_i)$ and $l_i^{\text{rev}}(\Theta) = -\log p_{\Theta}(x_i|y_i)$. Let $\alpha_{i,j}^{(t)} = -p_{\Theta_t}(v_j|v_i) + \delta_{i,j-n}$, $\beta_{i,j}^{(t)} = -p_{\Theta_t}(v_j|v_i) + \delta_{i-n,j}$. By [Lemma 5](#),

$$\begin{aligned} \frac{d\mathcal{L}(\Theta_t)}{dt} &= \left\langle \nabla \mathcal{L}(\Theta_t), \frac{d\Theta_t}{dt} \right\rangle = -\langle \nabla \mathcal{L}(\Theta_t), \nabla \mathcal{L}(\Theta_t) \rangle \\ &= -\left\| \frac{1}{2n-1} \left(\sum_{i=1}^n x_i (y_i - \mathbb{E}_{p_{\Theta_t}(\cdot|x_i)}[y])^\top + \sum_{i=2}^n y_i (x_i - \mathbb{E}_{p_{\Theta_t}(\cdot|y_i)}[x])^\top \right) \right\|^2 \\ &= -\left\| \frac{1}{2n-1} \left(\sum_{i=1}^n \sum_{j=1}^m \alpha_{i,j}^{(t)} v_i v_j^\top + \sum_{i=n+2}^{2n} \sum_{j=1}^m \beta_{i,j}^{(t)} v_i v_j^\top \right) \right\|^2. \end{aligned}$$

Similarly, we have

$$\begin{aligned}
& \frac{dl_i(\Theta_t)}{dt} \\
&= \left\langle \nabla l_i(\Theta_t), \frac{d\Theta_t}{dt} \right\rangle = - \langle \nabla l_i(\Theta_t), \nabla \mathcal{L}(\Theta_t) \rangle \\
&= - \left\langle x_i(y_i - \mathbb{E}_{p_{\Theta_t}(\cdot|x_i)}[y])^\top, \frac{1}{2n-1} \left(\sum_{i=1}^n x_i(y_i - \mathbb{E}_{p_{\Theta_t}(\cdot|x_i)}[y])^\top + \sum_{i=2}^n y_i(x_i - \mathbb{E}_{p_{\Theta_t}(\cdot|y_i)}[x])^\top \right) \right\rangle \\
&= - \left\langle \sum_{j=1}^m \alpha_{i,j} v_i v_j^\top, \frac{1}{2n-1} \left(\sum_{i=1}^n \sum_{j=1}^m \alpha_{i,j}^{(t)} v_i v_j^\top + \sum_{i=n+2}^{2n} \sum_{j=1}^m \beta_{i,j}^{(t)} v_i v_j^\top \right) \right\rangle,
\end{aligned}$$

and

$$\begin{aligned}
& \frac{dl_i^{\text{rev}}(\Theta_t)}{dt} \\
&= \left\langle \nabla l_i^{\text{rev}}(\Theta_t), \frac{d\Theta_t}{dt} \right\rangle = - \langle \nabla l_i^{\text{rev}}(\Theta_t), \nabla \mathcal{L}(\Theta_t) \rangle \\
&= - \left\langle y_i(x_i - \mathbb{E}_{p_{\Theta_t}(\cdot|y_i)}[x])^\top, \frac{1}{2n-1} \left(\sum_{i=1}^n x_i(y_i - \mathbb{E}_{p_{\Theta_t}(\cdot|x_i)}[y])^\top + \sum_{i=2}^n y_i(x_i - \mathbb{E}_{p_{\Theta_t}(\cdot|y_i)}[x])^\top \right) \right\rangle \\
&= - \left\langle \sum_{j=1}^m \beta_{i+n,j}^{(t)} v_{i+n} v_j^\top, \frac{1}{2n-1} \left(\sum_{i=1}^n \sum_{j=1}^m \alpha_{i,j}^{(t)} v_i v_j^\top + \sum_{i=n+2}^{2n} \sum_{j=1}^m \beta_{i,j}^{(t)} v_i v_j^\top \right) \right\rangle.
\end{aligned}$$

Applying [Lemma 7](#), with probability at least $1 - \delta/2$, for any $t \geq 0$ we have

$$\begin{aligned}
& \left| \frac{d\mathcal{L}(\Theta_t)}{dt} + \frac{1}{(2n-1)^2} \left(\sum_{i=1}^n \sum_{j=1}^m (\alpha_{i,j}^{(t)})^2 + \sum_{i=n+2}^{2n} \sum_{j=1}^m (\beta_{i,j}^{(t)})^2 \right) \right| \\
& \leq \epsilon \cdot \frac{1}{(2n-1)^2} \left(\sum_{i=1}^n \sum_{j=1}^m (\alpha_{i,j}^{(t)})^2 + \sum_{i=n+2}^{2n} \sum_{j=1}^m (\beta_{i,j}^{(t)})^2 \right),
\end{aligned} \tag{12}$$

and

$$\begin{aligned}
& \left| \frac{dl_i(\Theta_t)}{dt} + \frac{1}{2n-1} \sum_{j=1}^m (\alpha_{i,j}^{(t)})^2 \right| \\
& \leq \epsilon \cdot \frac{1}{2n-1} \left(\sum_{j=1}^m (\alpha_{i,j}^{(t)})^2 \right)^{1/2} \left(\sum_{i=1}^n \sum_{j=1}^m (\alpha_{i,j}^{(t)})^2 + \sum_{i=n+2}^{2n} \sum_{j=1}^m (\beta_{i,j}^{(t)})^2 \right)^{1/2}, \\
& \left| \frac{dl_i^{\text{rev}}(\Theta_t)}{dt} + \frac{1}{2n-1} \sum_{j=1}^m (\beta_{i+n,j}^{(t)})^2 \right| \\
& \leq \epsilon \cdot \frac{1}{2n-1} \left(\sum_{j=1}^m (\beta_{i+n,j}^{(t)})^2 \right)^{1/2} \left(\sum_{i=1}^n \sum_{j=1}^m (\alpha_{i,j}^{(t)})^2 + \sum_{i=n+2}^{2n} \sum_{j=1}^m (\beta_{i,j}^{(t)})^2 \right)^{1/2}.
\end{aligned} \tag{13}$$

Furthermore, [Lemma 6](#) implies that with probability at least $1 - \delta/2$

$$\frac{1}{2m} < p_{\Theta_0}(y_i|x_i), p_{\Theta_0}(x_i|y_i) < \frac{2}{m}. \quad (14)$$

The following arguments are based on the event that the above inequalities hold.

We first show that

$$\inf \{p_{\Theta_t}(x_i|y_i), p_{\Theta_t}(y_i|x_i) : t \geq 0, i \in [n]\} > \frac{1}{2m}.$$

We prove this by contradiction. Let

$$\tau = \inf \left\{ t \geq 0 : \exists i \in [n], \text{ s.t. } \min\{p_{\Theta_t}(y_i|x_i), p_{\Theta_t}(x_i|y_i)\} \leq \frac{1}{2m} \right\}.$$

By Eq. (14), it is obvious that $\tau > 0$. Assume without loss of generality that $p_{\Theta_\tau}(y_1|x_1) \leq \frac{1}{2m}$. It follows that there exists $\delta > 0$ such that $p_{\Theta_t}(y_1|x_1)$ is a decreasing function in $(\tau - \delta, \tau)$ and $p_{\Theta_t}(y_1|x_1) = \min\{p_{\Theta_t}(x_i|y_i), p_{\Theta_t}(y_i|x_i) : i \in [n]\}$ for any $t \in (\tau - \delta, \tau)$. It follows that for $t \in (\tau - \delta, \tau)$,

$$\begin{aligned} \frac{dl_1(\Theta_t)}{dt} &\leq \frac{1}{2n-1} \left(-\sum_{j=1}^m (\alpha_{1,j}^{(t)})^2 + \epsilon \cdot \left(\sum_{j=1}^m (\alpha_{1,j}^{(t)})^2 \right)^{1/2} \left(\sum_{i=1}^n \sum_{j=1}^m (\alpha_{i,j}^{(t)})^2 + \sum_{i=n+2}^{2n} \sum_{j=1}^m (\beta_{i,j}^{(t)})^2 \right)^{1/2} \right) \\ &\leq \frac{1}{2n-1} \left(-\sum_{j=1}^m (\alpha_{1,j}^{(t)})^2 + \epsilon \cdot \left(\sum_{j=1}^m (\alpha_{1,j}^{(t)})^2 \right)^{1/2} \left(2 \sum_{i=1}^n (\alpha_{i,i+n}^{(t)})^2 + 2 \sum_{i=n+2}^{2n} (\beta_{i,i-n}^{(t)})^2 \right)^{1/2} \right) \\ &\leq \frac{1}{2n-1} \left(\sum_{j=1}^m (\alpha_{1,j}^{(t)})^2 \right)^{1/2} \cdot \left(-\left(\sum_{j=1}^m (\alpha_{1,j}^{(t)})^2 \right)^{1/2} + \epsilon \cdot \left(4n(\alpha_{1,n+1}^{(t)})^2 \right)^{1/2} \right) \\ &\leq 0 \end{aligned}$$

where the first inequality is from Eq. (13); the second inequality is due to $\sum_{j \neq i+n} |\alpha_{i,j}^{(t)}| = \alpha_{i,i+n}^{(t)} = 1 - p_{\Theta_t}(y_i|x_i)$, $\sum_{j \neq i} |\beta_{i+n,j}^{(t)}| = \beta_{i+n,i}^{(t)} = 1 - p_{\Theta_t}(x_i|y_i)$ for all $i \in [n]$; the third inequality is because $p_{\Theta_t}(y_1|x_1) = \min\{p_{\Theta_t}(x_i|y_i), p_{\Theta_t}(y_i|x_i) : i \in [n]\}$. However, $p_{\Theta_t}(y_1|x_1)$ is a decreasing function in $(\tau - \delta, \tau)$, a contradiction. Therefore, we conclude that

$$\inf \{p_{\Theta_t}(x_i|y_i), p_{\Theta_t}(y_i|x_i) : t \geq 0, i \in [n]\} > \frac{1}{2m}.$$

Now we show

$$\mathcal{L}(\Theta_t) \leq \frac{1}{\frac{t}{8(2n-1)\log^2(2m)} + \frac{1}{\mathcal{L}(\Theta_0)}}, \quad \forall t \geq 0.$$

By Eq. (12),

$$\begin{aligned}
\frac{d\mathcal{L}(\Theta_t)}{dt} &\leq -\frac{1-\epsilon}{(2n-1)^2} \left(\sum_{i=1}^n \sum_{j=1}^m (\alpha_{i,j}^{(t)})^2 + \sum_{i=n+2}^{2n} \sum_{j=1}^m (\beta_{i,j}^{(t)})^2 \right) \\
&\leq -\frac{1-\epsilon}{(2n-1)^2} \left(\sum_{i=1}^n (1-p_{\Theta_t}(y_i|x_i))^2 + \sum_{i=2}^n (1-p_{\Theta_t}(x_i|y_i))^2 \right) \\
&\leq -\frac{1-\epsilon}{(2n-1)^3} \left(\sum_{i=1}^n (1-p_{\Theta_t}(y_i|x_i)) + \sum_{i=2}^n (1-p_{\Theta_t}(x_i|y_i)) \right)^2 \\
&\leq -\frac{1-\epsilon}{8(2n-1)\log^2(2m)} \mathcal{L}(\Theta_t)^2 \\
&\leq -\frac{1}{8(2n-1)\log^2(2m)} \mathcal{L}(\Theta_t)^2,
\end{aligned}$$

where the second inequality is due to $\sum_{j \neq i+n} |\alpha_{i,j}^{(t)}| = \alpha_{i,i+n}^{(t)} = 1 - p_{\Theta_t}(y_i|x_i)$, $\sum_{j \neq i} |\beta_{i+n,j}^{(t)}| = \beta_{i+n,i}^{(t)} = 1 - p_{\Theta_t}(x_i|y_i)$ for all $i \in [n]$; the third inequality applies Cauchy-Schwarz inequality; the last inequality uses the fact that $p_{\Theta_t}(x_i|y_i), p_{\Theta_t}(y_i|x_i) > \frac{1}{2m}$ for any $t \geq 0, i \in [n]$ and the inequality $1-x \geq \frac{\log x}{2\log(1/(2m))}$ for $x \in (\frac{1}{2m}, 1)$.

By Lemma 10, we conclude that $\forall t \geq 0$,

$$\mathcal{L}(\Theta_t) \leq \frac{1}{\frac{t}{8(2n-1)\log^2(2m)} + \frac{1}{\mathcal{L}(\Theta_0)}},$$

which completes the proof. \square

Lemma 4 (Dynamics of the reversal loss). *Let $x_1, \dots, x_n, y_1, \dots, y_n, \mathcal{L}^{\text{rev}}(\Theta)$, and Θ_t ($t \geq 0$) be defined as in Theorem 5. When $\sigma \leq \frac{1}{100 \ln(16n^2/\delta)}$ and $d \geq 400n^2m^2 \log(8m^2n^2/\delta)/\epsilon^2$, with probability at least $1 - \delta$,*

$$\mathcal{L}^{\text{rev}}(\Theta_t) \geq \mathcal{L}^{\text{rev}}(\Theta_0) \cdot \left(1 + \frac{\mathcal{L}(\Theta_0) \cdot t}{8(2n-1)\log^2(2m)} \right)^{-8\epsilon(2n-1)\log^2(2m)}.$$

Proof. Similar to Lemma 3, we assume $x_1, \dots, x_n = v_1, \dots, v_n$ and $y_1, \dots, y_n = v_{n+1}, \dots, v_{2n}$ WLOG. Let $\alpha_{i,j}^{(t)} = -p_{\Theta_t}(v_j|v_i) + \delta_{i,j-n}, \beta_{i,j}^{(t)} = -p_{\Theta_t}(v_j|v_i) + \delta_{i-n,j}$. By Lemma 5,

$$\begin{aligned}
&\frac{d\mathcal{L}^{\text{rev}}(\Theta_t)}{dt} \\
&= \left\langle \nabla \mathcal{L}^{\text{rev}}(\Theta_t), \frac{d\Theta_t}{dt} \right\rangle \\
&= - \left\langle y_1(x_1 - \mathbb{E}_{p_{\Theta_t}(\cdot|y_1)}[x])^\top, \frac{1}{2n-1} \left(\sum_{i=1}^n x_i(y_i - \mathbb{E}_{p_{\Theta_t}(\cdot|x_i)}[y])^\top + \sum_{i=2}^n y_i(x_i - \mathbb{E}_{p_{\Theta_t}(\cdot|y_i)}[x])^\top \right) \right\rangle \\
&= - \left\langle \sum_{j=1}^m \beta_{n+1,j}^{(t)} v_{n+1} v_j^\top, \frac{1}{2n-1} \left(\sum_{i=1}^n \sum_{j=1}^m \alpha_{i,j}^{(t)} v_i v_j^\top + \sum_{i=n+2}^{2n} \sum_{j=1}^m \beta_{i,j}^{(t)} v_i v_j^\top \right) \right\rangle.
\end{aligned}$$

Applying [Lemma 7](#), with probability at least $1 - \delta/2$, for any $t \geq 0$ we have

$$\left| \frac{d\mathcal{L}^{\text{rev}}(\Theta_t)}{dt} \right| \leq \epsilon \cdot \frac{1}{2n-1} \left(\sum_{j=1}^m (\beta_{n+1,j}^{(t)})^2 \right)^{1/2} \left(\sum_{i=1}^n \sum_{j=1}^m (\alpha_{i,j}^{(t)})^2 + \sum_{i=n+2}^{2n} \sum_{j=1}^m (\beta_{i,j}^{(t)})^2 \right)^{1/2}, \quad (15)$$

and

$$\begin{aligned} & \left| \frac{d\mathcal{L}(\Theta_t)}{dt} + \frac{1}{(2n-1)^2} \left(\sum_{i=1}^n \sum_{j=1}^m (\alpha_{i,j}^{(t)})^2 + \sum_{i=n+2}^{2n} \sum_{j=1}^m (\beta_{i,j}^{(t)})^2 \right) \right| \\ & \leq \epsilon \cdot \frac{1}{(2n-1)^2} \left(\sum_{i=1}^n \sum_{j=1}^m (\alpha_{i,j}^{(t)})^2 + \sum_{i=n+2}^{2n} \sum_{j=1}^m (\beta_{i,j}^{(t)})^2 \right), \end{aligned}$$

as well as

$$\begin{aligned} & \left| \frac{dl_i(\Theta_t)}{dt} + \frac{1}{2n-1} \sum_{j=1}^m (\alpha_{i,j}^{(t)})^2 \right| \\ & \leq \epsilon \cdot \frac{1}{2n-1} \left(\sum_{j=1}^m (\alpha_{i,j}^{(t)})^2 \right)^{1/2} \left(\sum_{i=1}^n \sum_{j=1}^m (\alpha_{i,j}^{(t)})^2 + \sum_{i=n+2}^{2n} \sum_{j=1}^m (\beta_{i,j}^{(t)})^2 \right)^{1/2}, \\ & \left| \frac{dl_i^{\text{rev}}(\Theta_t)}{dt} + \frac{1}{2n-1} \sum_{j=1}^m (\beta_{i+n,j}^{(t)})^2 \right| \\ & \leq \epsilon \cdot \frac{1}{2n-1} \left(\sum_{j=1}^m (\beta_{i+n,j}^{(t)})^2 \right)^{1/2} \left(\sum_{i=1}^n \sum_{j=1}^m (\alpha_{i,j}^{(t)})^2 + \sum_{i=n+2}^{2n} \sum_{j=1}^m (\beta_{i,j}^{(t)})^2 \right)^{1/2}. \end{aligned}$$

Furthermore, [Lemma 6](#) implies that with probability at least $1 - \delta/2$,

$$\frac{1}{2m} \leq p_{\Theta_0}(y_i|x_i), p_{\Theta_0}(x_i|y_i) \leq \frac{2}{m}. \quad (16)$$

The following arguments are based on the event that the above inequalities hold.

By Eq. (15),

$$\frac{d\mathcal{L}^{\text{rev}}(\Theta_t)}{dt} \geq -\epsilon \cdot \frac{1}{2n-1} \underbrace{\left(\sum_{j=1}^m (\beta_{n+1,j}^{(t)})^2 \right)}_{A_t}^{1/2} \underbrace{\left(\sum_{i=1}^n \sum_{j=1}^m (\alpha_{i,j}^{(t)})^2 + \sum_{i=n+2}^{2n} \sum_{j=1}^m (\beta_{i,j}^{(t)})^2 \right)}_{B_t}^{1/2}.$$

Notice that

$$\begin{aligned}
B_t &\leq 2 \sum_{i=1}^n (1 - p_{\Theta_t}(y_i|x_i))^2 + 2 \sum_{i=2}^n (1 - p_{\Theta_t}(x_i|y_i))^2 \\
&\leq 2 \left(\sum_{i=1}^n (1 - p_{\Theta_t}(y_i|x_i)) + \sum_{i=2}^n (1 - p_{\Theta_t}(x_i|y_i)) \right)^2 \\
&\leq 2(2n-1)^2 \mathcal{L}(\Theta_t)^2 \\
&\leq 2(2n-1)^2 \left(\frac{1}{\frac{t}{8(2n-1)\log^2(2m)} + \frac{1}{\mathcal{L}(\Theta_0)}} \right)^2
\end{aligned}$$

where the first inequality uses $\sum_{j \neq i+n} |\alpha_{i,j}^{(t)}| = \alpha_{i,i+n}^{(t)} = 1 - p_{\Theta_t}(y_i|x_i)$, $\sum_{j \neq i} |\beta_{i+n,j}^{(t)}| = \beta_{i+n,i}^{(t)} = 1 - p_{\Theta_t}(x_i|y_i)$ for all $i \in [n]$; the third inequality uses the fact that $1 - x \leq -\log x$; the last inequality applies [Lemma 3](#).

Similarly,

$$A_t \leq 2(1 - p_{\Theta_t}(x_1|y_1))^2 \leq 2\mathcal{L}^{\text{rev}}(\Theta_t)^2.$$

Combining, we have

$$\begin{aligned}
\frac{d\mathcal{L}^{\text{rev}}(\Theta_t)}{dt} &\geq -\epsilon \cdot \frac{1}{2n-1} \cdot 2\mathcal{L}^{\text{rev}}(\Theta_t) \cdot (2n-1) \cdot \frac{1}{\frac{t}{8(2n-1)\log^2(2m)} + \frac{1}{\mathcal{L}(\Theta_0)}} \\
&\geq -8\epsilon(2n-1)\log^2(2m) \cdot \mathcal{L}^{\text{rev}}(\Theta_t) \cdot \frac{1}{t + \frac{8(2n-1)\log^2(2m)}{\mathcal{L}(\Theta_0)}}.
\end{aligned}$$

By [Lemma 10](#), we conclude that $\forall t \geq 0$,

$$\mathcal{L}^{\text{rev}}(\Theta_t) \geq \mathcal{L}^{\text{rev}}(\Theta_0) \cdot \left(1 + \frac{\mathcal{L}(\Theta_0) \cdot t}{8(2n-1)\log^2(2m)} \right)^{-8\epsilon(2n-1)\log^2(2m)},$$

This completes the proof. □

Lemma 5 (Gradient of the loss function). *Define*

$$\begin{aligned}
\mathcal{L}(\Theta) &= \frac{1}{2n-1} \left(\sum_{i=1}^n -\log p_{\Theta}(y_i|x_i) + \sum_{i=2}^n -\log p_{\Theta}(x_i|y_i) \right), \\
\mathcal{L}^{\text{rev}}(\Theta) &= -\log p_{\Theta}(x_1|y_1).
\end{aligned}$$

Then we have

$$\begin{aligned}
\nabla \mathcal{L}(\Theta) &= -\frac{1}{2n-1} \left(\sum_{i=1}^n x_i(y_i - \mathbb{E}_{p_{\Theta}(\cdot|x_i)}[y])^\top + \sum_{i=2}^n y_i(x_i - \mathbb{E}_{p_{\Theta}(\cdot|y_i)}[x])^\top \right), \\
\nabla \mathcal{L}^{\text{rev}}(\Theta) &= -y_1(x_1 - \mathbb{E}_{p_{\Theta}(\cdot|y_1)}[x])^\top.
\end{aligned}$$

Proof. We have

$$\begin{aligned}
& \nabla(-\log p_{\Theta}(y|x)) \\
&= -\frac{\nabla p_{\Theta}(y|x)}{p_{\Theta}(y|x)} \\
&= -\frac{1}{p_{\Theta}(y|x)} \cdot \frac{xy^{\top} \exp(x^{\top} \Theta y) \left(\sum_{y \in \mathcal{V}} \exp(x^{\top} \Theta y) \right) - \exp(x^{\top} \Theta y) \left(\sum_{y \in \mathcal{V}} xy^{\top} \exp(x^{\top} \Theta y) \right)}{\left(\sum_{y \in \mathcal{V}} \exp(x^{\top} \Theta y) \right)^2} \\
&= -\frac{1}{p_{\Theta}(y|x)} \left(p_{\Theta}(y|x) xy^{\top} - p_{\Theta}(y|x) \sum_{y \in \mathcal{V}} p_{\Theta}(y|x) xy^{\top} \right) \\
&= -x \left(y - \sum_{y \in \mathcal{V}} p_{\Theta}(y|x) y \right)^{\top} \\
&= -x \left(y - \mathbb{E}_{y \sim p_{\Theta}(\cdot|x)}[y] \right)^{\top}.
\end{aligned}$$

The statements follow immediately. \square

A.2 Initialization

Lemma 6 (Initial distributions are all close to uniform). *Fix any $\delta \in (0, 1)$. Let $x_1, x_2, \dots, x_n \stackrel{i.i.d.}{\sim} \mathcal{N}_d(\mathbf{0}_d, \frac{1}{d} I_d)$. Let $\Theta \in \mathbb{R}^{d \times d}$, where each $\Theta_{ij} \stackrel{i.i.d.}{\sim} \mathcal{N}(0, \sigma^2)$ independent of x_1, \dots, x_n . For any $i, j \in [n]$, define*

$$p_{\Theta}(x_j|x_i) = \frac{\exp(l_{\Theta}(x_j|x_i))}{\sum_{k=1}^n \exp(l_{\Theta}(x_k|x_i))}, \quad \text{where } l_{\Theta}(x_j|x_i) = x_i^{\top} \Theta x_j.$$

Then when $\sigma^2 \leq \frac{1}{100 \ln(4n^2/\delta)}$ and $d \geq 400 \log(1/(2\delta n^2))/\epsilon^2$, with probability at least $1 - \delta$,

$$|p_{\Theta}(x_j|x_i) - 1/n| \leq \frac{1}{2n}, \quad \forall i, j \in [n].$$

Proof. Let $v = 0.2$. By [Lemma 8](#), with probability at least $1 - \delta$, we have

$$|\langle x_i, x_j \rangle - \delta_{ij}| \leq v, \quad \forall i, j \in [n].$$

Conditioned on the above high-probability event, we can further obtain that for any $j \in [n]$

$$p_{\Theta}(x_j|x_i) = \frac{\exp(l_{\Theta}(x_j|x_i))}{\sum_{k=1}^n \exp(l_{\Theta}(x_k|x_i))} \leq \frac{\exp(v)}{\sum_{k=1}^n \exp(-v)} = \frac{\exp(2v)}{n},$$

and

$$p_{\Theta}(x_j|x_i) = \frac{\exp(l_{\Theta}(x_j|x_i))}{\sum_{k=1}^n \exp(l_{\Theta}(x_k|x_i))} \geq \frac{\exp(-v)}{\sum_{k=1}^n \exp(v)} = \frac{\exp(-2v)}{n},$$

It follows that

$$\frac{1}{2n} < p_{\Theta}(x_j|x_i) < \frac{3}{2n} \implies |p_{\Theta}(x_j|x_i) - 1/n| < \frac{1}{2n}.$$

which completes the proof. \square

A.3 Subspace embedding

Lemma 7 (ℓ_1 -subspace embedding of Gaussian second-order tensors). *Let z_1, \dots, z_n be independently sampled from $\mathcal{N}_d(\mathbf{0}_d, \frac{1}{d}I_d)$. Let $\mathcal{I}_1, \mathcal{I}_2 \subseteq [n] \times [n]$ be two index sets. Let $\mathcal{I}_0 = \mathcal{I}_1 \cap \mathcal{I}_2$. If $d \geq 64 \log(2n^2/\delta)/\epsilon^2$, then with probability at least $1 - \delta$,*

$$\left| \left\langle \sum_{(i,j) \in \mathcal{I}_1} \alpha_{i,j} z_i z_j^\top, \sum_{(i,j) \in \mathcal{I}_2} \beta_{i,j} z_i z_j^\top \right\rangle - \sum_{(i,j) \in \mathcal{I}_0} \alpha_{i,j} \beta_{i,j} \right| \leq \epsilon \cdot \left(\sum_{(i,j) \in \mathcal{I}_1} |\alpha_{i,j}| \right) \left(\sum_{(i,j) \in \mathcal{I}_2} |\beta_{i,j}| \right)$$

holds for any $\alpha_{i,j}, \beta_{i,j}$. Furthermore, if $d \geq 64k^2 \log(2n^2/\delta)/\epsilon^2$, then with probability at least $1 - \delta$,

$$\left| \left\langle \sum_{(i,j) \in \mathcal{I}_1} \alpha_{i,j} z_i z_j^\top, \sum_{(i,j) \in \mathcal{I}_2} \beta_{i,j} z_i z_j^\top \right\rangle - \sum_{(i,j) \in \mathcal{I}_0} \alpha_{i,j} \beta_{i,j} \right| \leq \epsilon \cdot \left(\sum_{(i,j) \in \mathcal{I}_1} \alpha_{i,j}^2 \right)^{1/2} \left(\sum_{(i,j) \in \mathcal{I}_2} \beta_{i,j}^2 \right)^{1/2}$$

holds for any $\alpha_{i,j}, \beta_{i,j}$ such that $\|\alpha\|_0 \leq k, \|\beta\|_0 \leq k$.

Proof. Using Lemma 8 and Cauchy-Schwarz inequality, we have

$$\begin{aligned} & \left| \left\langle \sum_{(i,j) \in \mathcal{I}_1} \alpha_{i,j} z_i z_j^\top, \sum_{(i,j) \in \mathcal{I}_2} \beta_{i,j} z_i z_j^\top \right\rangle - \sum_{(i,j) \in \mathcal{I}_0} \alpha_{i,j} \beta_{i,j} \right| \\ & \leq \left| \sum_{(i,j) \in \mathcal{I}_0} \alpha_{i,j} \beta_{i,j} (\|z_i\|^2 \|z_j\|^2 - 1) + \sum_{(i,j) \in \mathcal{I}_1, (k,l) \in \mathcal{I}_2, (i,j) \neq (k,l)} \alpha_{i,j} \beta_{k,l} z_i^\top z_k z_j^\top z_l \right| \\ & \leq \sqrt{\frac{64 \log(2n^2/\delta)}{d}} \cdot \left(\sum_{(i,j) \in \mathcal{I}} |\alpha_{i,j} \beta_{i,j}| + \sum_{(i,j) \in \mathcal{I}_1, (k,l) \in \mathcal{I}_2, (i,j) \neq (k,l)} |\alpha_{i,j} \beta_{k,l}| \right) \\ & = \sqrt{\frac{64 \log(2n^2/\delta)}{d}} \cdot \left(\sum_{(i,j) \in \mathcal{I}_1} |\alpha_{i,j}| \right) \cdot \left(\sum_{(i,j) \in \mathcal{I}_2} |\beta_{i,j}| \right) \\ & \leq \sqrt{\frac{64k^2 \log(2n^2/\delta)}{d}} \cdot \left(\sum_{(i,j) \in \mathcal{I}_1} \alpha_{i,j}^2 \right)^{1/2} \left(\sum_{(i,j) \in \mathcal{I}_2} \beta_{i,j}^2 \right)^{1/2}. \end{aligned}$$

The statements follow directly from plugging in suitable values of d . \square

Lemma 8 (Almost orthonormal). *Let $x_1, x_2, \dots, x_n \stackrel{i.i.d.}{\sim} \mathcal{N}_d(\mathbf{0}_d, \frac{1}{d}I_d)$. For any $\epsilon, \delta \in (0, 1)$, when $d \geq 16 \log(2n^2/\delta)/\epsilon^2$, it holds that with probability at least $1 - \delta$,*

$$|\langle x_i, x_j \rangle - \delta_{ij}| \leq \epsilon, \quad \forall i, j \in [n].$$

Proof. Fix $i \neq j \in [n]$. Notice

$$\begin{aligned} |\langle x_i, x_j \rangle| &= |\langle x_i + x_j, x_i + x_j \rangle - \langle x_i - x_j, x_i - x_j \rangle|/4 \\ &\leq (|\langle x_i + x_j, x_i + x_j \rangle - 1| + |\langle x_i - x_j, x_i - x_j \rangle - 1|)/4. \end{aligned}$$

Using Lemma 9, we have that with probability at least $1 - \delta/n^2$,

$$|\langle x_i, x_j \rangle| \leq \epsilon.$$

Furthermore, fix $i \in [n]$, with probability at least $1 - \delta/n^2$,

$$|\langle x_i, x_i \rangle - 1| \leq \epsilon.$$

The statement then follows from union bound over $i, j \in [n]$. \square

Lemma 9 (Almost normal for a fixed vector). *For a d -dimensional random vector $x \sim \mathcal{N}_d(\mathbf{0}_d, \frac{1}{d}I_d)$ and any $v \in (0, 1/2)$,*

$$\mathbb{P}(|\langle x, x \rangle - 1| \geq v) \leq 2e^{-v^2 d/16}.$$

In particular, when $d \geq 16 \log(1/(2\delta))/v^2$, we have

$$\mathbb{P}(|\langle x, x \rangle - 1| \geq v) \leq \delta$$

Proof. Let $x = (x_1, \dots, x_d)$. By [Lemma 11](#) (letting $x = v^2 d/16$),

$$\begin{aligned} \mathbb{P}(|\langle x, x \rangle - 1| \geq v) &\leq \mathbb{P}\left(\left|\sum_{i=1}^d (\sqrt{d} \cdot x_i)^2 - d\right| \geq vd\right) \\ &\leq 2e^{-v^2 d/16}. \end{aligned}$$

The second inequality follows from simple arithmetics. \square

A.4 Useful results

Lemma 10 (ODE bound). *Let $c_1, c_2, c_3 > 0$. Suppose the function $f_1, f_2 : \mathbb{R}_+ \rightarrow \mathbb{R}$ satisfies $f_1(0) > 0, f_2(0) > 0$ and*

$$\begin{aligned} \frac{df_1(t)}{dt} &\leq -c_1 \cdot f_1(t)^2, \\ \frac{df_2(t)}{dt} &\geq -c_2 \cdot f_2(t) \cdot \frac{1}{t + c_3}. \end{aligned}$$

Then

$$\begin{aligned} f_1(t) &\leq \frac{1}{c_1 t + \frac{1}{f_1(0)}}, \\ f_2(t) &\geq f_2(0) \cdot \left(1 + \frac{t}{c_3}\right)^{-c_2}. \end{aligned}$$

Proof. The conditions imply that

$$\begin{aligned} \frac{df_1^{-1}(t)}{dt} &= -\frac{1}{f_1^2(t)} \cdot \frac{df_1(t)}{dt} \geq c_1, \\ \frac{d \log f_2(t)}{dt} &= \frac{1}{f_2(t)} \cdot \frac{df_2(t)}{dt} \geq -c_2/(t + c_3). \end{aligned}$$

It follows that

$$\begin{aligned} f_1^{-1}(t) &\geq c_1 t + f_1^{-1}(0), \\ \log f_2(t) &\geq -c_2 \log(1 + t/c_3) + \log f_2(0). \end{aligned}$$

Rearranging the above inequalities, one can obtain the desired results. \square

Lemma 11 (χ^2 -concentration bound, Lemma 1 of [Laurent and Massart \(2000\)](#)). *Let g_1, \dots, g_t be i.i.d. $\mathcal{N}(0, 1)$ random variables. Then for any $x \geq 0$,*

$$\Pr \left[\sum_{i=1}^t g_i^2 \geq t + 2\sqrt{tx} + 2x \right] \leq \exp(-x),$$

and

$$\Pr \left[\sum_{i=1}^t g_i^2 \leq t - 2\sqrt{tx} \right] \leq \exp(-x).$$

B Missing Proofs of [Section 4](#)

In this section, we show missing proofs in [Section 4](#).

B.1 Proofs of [Section 4.1](#)

B.1.1 Proofs of [Proposition 4.1](#) and [Proposition 4.2](#)

We first show the proofs of [Proposition 4.1](#) and [Proposition 4.2](#), respectively.

Proof of [Proposition 4.1](#). Actually, for any three tokens x_1, x_2, x_3 , it holds that

$$p_{\theta(0)}(x_3|x_1, x_2) = \frac{\exp(\mathbf{x}_3^\top Y(0)^\top \text{LN}(X^\top \mathbf{b}_2))}{\sum_{x' \in [M]} \exp(\mathbf{x}'^\top Y(0)^\top \text{LN}(X^\top \mathbf{b}_2))} = \frac{\exp(0)}{\sum_{x' \in [M]} \exp(0)} = 1/M,$$

since $Y(0) = \mathbf{0}$. □

Proof of [Proposition 4.2](#). Note that the input sequence length $T = 2$. By [\(8\)](#),

$$p_{\theta(t)}(x|x_1, x_2) = \frac{\exp(\mathbf{x}^\top Y(t)^\top \text{LN}(X^\top \mathbf{b}_2))}{\sum_{x' \in [M]} \exp(\mathbf{x}'^\top Y(t)^\top \text{LN}(X^\top \mathbf{b}_2))}$$

where $\mathbf{b}_2 = [b_{12}]$ and $b_{12} = 1$ by [\(7\)](#). Also, $X = [\mathbf{x}_1]^\top$ is a one-hot row vector. Therefore, $\text{LN}(X^\top \mathbf{b}_2) = \text{LN}(\mathbf{x}_1 b_{12}) = \text{LN}(\mathbf{x}_1) = \mathbf{x}_1$, and thus

$$p_{\theta(t)}(x|x_1, x_2) = \frac{\exp(\mathbf{x}^\top Y(t)^\top \mathbf{x}_1)}{\sum_{x' \in [M]} \exp(\mathbf{x}'^\top Y(t)^\top \mathbf{x}_1)} = \frac{\exp(Y(t)_{x_1, x})}{\sum_{x' \in [M]} \exp(Y(t)_{x_1, x'})}$$

where $Y(t)_{i,j}$ is the entry of the matrix $Y(t)$ at row i and column j . □

B.1.2 Proof of [Lemma 2](#)

Proof of [Lemma 2](#). We first calculate the gradient of Y when the current batch is a sequence (x_1, x_2, x_3) . Note that the input sequence length $T = 2$ and by the proof of [Proposition 4.2](#), we have $\text{LN}(X^\top \mathbf{b}_T) = \text{LN}(X^\top \mathbf{b}_2) = \mathbf{x}_1$. By [Lemma 1](#), we have

$$\dot{Y} = \eta_Y \text{LN}(X^\top \mathbf{b}_T) (\mathbf{x}_{T+1} - \boldsymbol{\alpha})^\top = \eta_Y \mathbf{x}_1 (\mathbf{x}_3 - \boldsymbol{\alpha})^\top$$

where $\boldsymbol{\alpha} = [\alpha_1, \alpha_2, \dots, \alpha_M]^\top \in \mathbb{R}^M$ with $\boldsymbol{\alpha} = \exp(Y_{x_1}^\top) / \mathbf{1}^\top \exp(Y_{x_1}^\top)$. Note that $\mathbf{x}_1(\mathbf{x}_3 - \boldsymbol{\alpha})^\top$ is a matrix with only x_1 -th row non-zero since \mathbf{x}_1 is one-hot. Therefore, the update of each row of Y are independent and only x_1 -th row of Y gets updated at the current time step.

Now we consider any fixed $x_1 \in \mathcal{V}$. Let $t_{x_1, i}$ be the time step that the x_1 -th row of Y gets updated (i.e., the first token of the training data is x_1 for the current batch) for the i -th time and let $t_{x_1, 0} = 0$ for notation convenience, then

$$Y(t_{x_1, i})_{x_1} = Y(t_{x_1, i-1})_{x_1} + \eta_Y(\mathbf{x}_3 - \boldsymbol{\alpha})^\top.$$

For convenience, we denote $\mathbf{y}(i) = Y(t_{x_1, i})_{x_1}^\top$, and thus

$$\mathbf{y}(i) = \mathbf{y}(i-1) + \eta_Y(\mathbf{x}_3 - \boldsymbol{\alpha}(i-1)) \quad (17)$$

where $\mathbf{y}(0) = \mathbf{0}$ and $\boldsymbol{\alpha}(i-1) = \exp(\mathbf{y}(i-1)) / \mathbf{1}^\top \exp(\mathbf{y}(i-1))$. Note that for a fixed x_1 , x_3 is also fixed by our construction of the dataset. By Lemma 5 of Tian et al. (2023a), we can obtain that

$$\mathbf{y}(i) = (M-1)h^*(i)\boldsymbol{\xi}_{x_3},$$

where $\boldsymbol{\xi}_{x_3} = \frac{M}{M-1}(\mathbf{x}_3 - \frac{1}{M}\mathbf{1})$ and $h^*(i)$ can be derived recursively as

$$h^*(i) = h^*(i-1) + \frac{\eta_Y}{(M-1) + \exp(Mh^*(i-1))}$$

with $h^*(0) = 0$. Combining Lemma 7 and 9 in Tian et al. (2023a), we have

$$h^*(i) \gtrsim \frac{1}{M} \ln(M\eta_Y i), \quad \forall i \gtrsim \frac{\ln M}{\eta_Y}. \quad (18)$$

Note that the update of each row of Y are independent, the training set has size N , and the batch size is 1, we have

$$Y(t)_{x_1}^\top = (M-1)h^*([t/N])\boldsymbol{\xi}_{x_3}$$

where the training data at time step t is (x_1, x_2, x_3) . Combining (18), we can obtain that

$$Y(t)_{x_1, x_3} \gtrsim (M-1) \cdot \frac{M}{M-1} \left(1 - \frac{1}{M}\right) \cdot \frac{1}{M} \ln(M\eta_Y [t/N]) \geq \ln\left(\frac{M\eta_Y t}{N}\right)$$

and

$$Y(t)_{x_1, x} \lesssim (M-1) \cdot \frac{M}{M-1} \left(-\frac{1}{M}\right) \cdot \frac{1}{M} \ln(M\eta_Y [t/N]) \leq -\frac{1}{M} \ln\left(\frac{M\eta_Y t}{N}\right), \quad \forall x \neq x_3.$$

On the other hand, for any sequence (x_1, x_2, x_3) in the test set, since the x_1 -th row of Y has never been updated, we have

$$Y(t)_{x_1, x} = Y(0)_{x_1, x} = 0, \quad \forall x \in [M].$$

□

B.1.3 Proof of Theorem 3

Proof. We first consider training sequence (x_1, x_2, x_3) at time t . By Proposition 4.2, we have

$$p_{\theta(t)}(x_3|x_1, x_2) = \frac{\exp(Y(t)_{x_1, x_3})}{\sum_{x' \in [M]} \exp(Y(t)_{x_1, x'})}$$

and by Lemma 2, we have

$$Y(t)_{x_1, x_3} \geq c \ln \left(\frac{M\eta_Y t}{N} \right), \quad \text{and} \quad Y(t)_{x_1, x} \leq -\frac{c}{M} \ln \left(\frac{M\eta_Y t}{N} \right), \quad \forall x \neq x_3$$

for some constant $c > 0$. Therefore,

$$\begin{aligned} p_{\theta(t)}(x_3|x_1, x_2) &\geq \frac{\exp \left(c \ln \left(\frac{M\eta_Y t}{N} \right) \right)}{\exp \left(c \ln \left(\frac{M\eta_Y t}{N} \right) \right) + (M-1) \ln \left(-\frac{c}{M} \ln \left(\frac{M\eta_Y t}{N} \right) \right)} \\ &\geq \frac{\left(\frac{M\eta_Y t}{N} \right)^c}{\left(\frac{M\eta_Y t}{N} \right)^c + (M-1)} \\ &= 1 - \frac{M-1}{\left(\frac{M\eta_Y t}{N} \right)^c + (M-1)} \\ &\geq 1 - \frac{M-1}{2 \left(\frac{M\eta_Y t}{N} \right)^c} \end{aligned}$$

where the last inequality holds since

$$\ln t \gtrsim \ln(NM/\eta_Y) \implies t \geq \frac{N(M-1)^{1/c}}{M\eta_Y} \implies \left(\frac{M\eta_Y t}{N} \right)^c \geq M-1.$$

Finally, for any sequence $(x_1, x_2, x_3) \in \mathcal{D}_{\text{test}}$, since $Y(t)_{x_1, x} = 0, \forall x \in [M]$ according to Lemma 2, we have

$$p_{\theta(t)}(x_3|x_1, x_2) = \frac{\exp(Y(t)_{x_1, x_3})}{\sum_{x' \in [M]} \exp(Y(t)_{x_1, x'})} = \frac{\exp(0)}{M \cdot \exp(0)} = 1/M,$$

which completes the proof. \square

B.2 Proof of Section 4.2

Proof of Theorem 4. Recall that by Proposition 4.2, we have

$$p_{\theta(t)}(x_3|x_1, x_2) = \frac{\exp(Y(t)_{x_1, x_3})}{\sum_{x' \in [M]} \exp(Y(t)_{x_1, x'})}$$

and by Lemma 2, we have

$$Y(t)_{\mathbf{A}_i, \mathbf{B}_i} \geq c \ln \left(\frac{M\eta_Y t}{N} \right), \quad \text{and} \quad Y(t)_{\mathbf{A}_i, x} \leq -\frac{c}{M} \ln \left(\frac{M\eta_Y t}{N} \right), \quad \forall x \neq \mathbf{B}_i$$

for some constant $c > 0$. Therefore, using the same proof as [Theorem 3](#), we have

$$p_{\theta(t)}(\mathbf{B}_i | \mathbf{A}_i \rightarrow) \geq 1 - \frac{M-1}{2 \left(\frac{M\eta_Y t}{N} \right)^c}.$$

Additionally, according to the proof of [Lemma 2](#), $Y(t)_{\mathbf{A}_i, x}$ has the same value across all $x \neq \mathbf{B}_i$, which implies

$$p_{\theta(t)}(\mathbf{C}_i | \mathbf{A}_i \rightsquigarrow) \leq \frac{1}{M}.$$

Similarly, applying [Lemma 2](#) to $Y(t)_{\mathbf{B}_i}$, we can obtain that

$$p_{\theta(t)}(\mathbf{C}_i | \mathbf{B}_i \rightarrow) \geq 1 - \frac{M-1}{2 \left(\frac{M\eta_Y t}{N} \right)^c}.$$

□

C Additional Experimental Results

In this section, we show additional experimental results for [Section 5](#).

C.1 Details of model architectures and hyperparameters

For both the reversal curse and COT experiments, we used the GPT2 model architecture and trained the model with the AdamW optimizer for 3000 epochs of batch size 64. See [Table 2](#) for a full list of hyperparameters. We also conducted experiments under various model configurations and vocabulary sizes to show that the results in [Sections 5.1](#) and [5.2](#) are consistent under different settings. See [Table 3](#) for a complete list of different configurations, where the default choices are boldened.

Parameters	Values
Learning Rate	0.01
Weight Decay λ	0.9
(β_1, β_2)	(0.9, 0.999)
Batch Size	64
Number of Epochs	3000

Table 2: Full list of hyperparameters for AdamW optimizer and training.

C.2 Additional experimental results for reversal curse

In this section, we show additional experimental results for the reversal curse under different configurations, including different vocabulary sizes ([Figure 5](#)), different number of layers ([Figure 6](#)), different positional encoding ([Figure 7](#)), different entity lengths ([Figure 8](#)) and whether token and positional embeddings are trainable or fixed ([Figure 9](#)). Note that our experimental results consistently show the reversal curse happens under different settings.

Parameters	Values
Number of Layers	12, 24 , 48
Number of Heads	12
Vocabulary Size	20, 50, 200, 800 , 2000
Entity Length	1 , 2, 3
Positional Encoding Type	None, Absolute , Relative
Token, Positional Embedding	Learnable , Frozen

Table 3: The list of different configurations for experiments in [Appendices C.2](#) and [C.3](#). Default choices are bolded for each row.

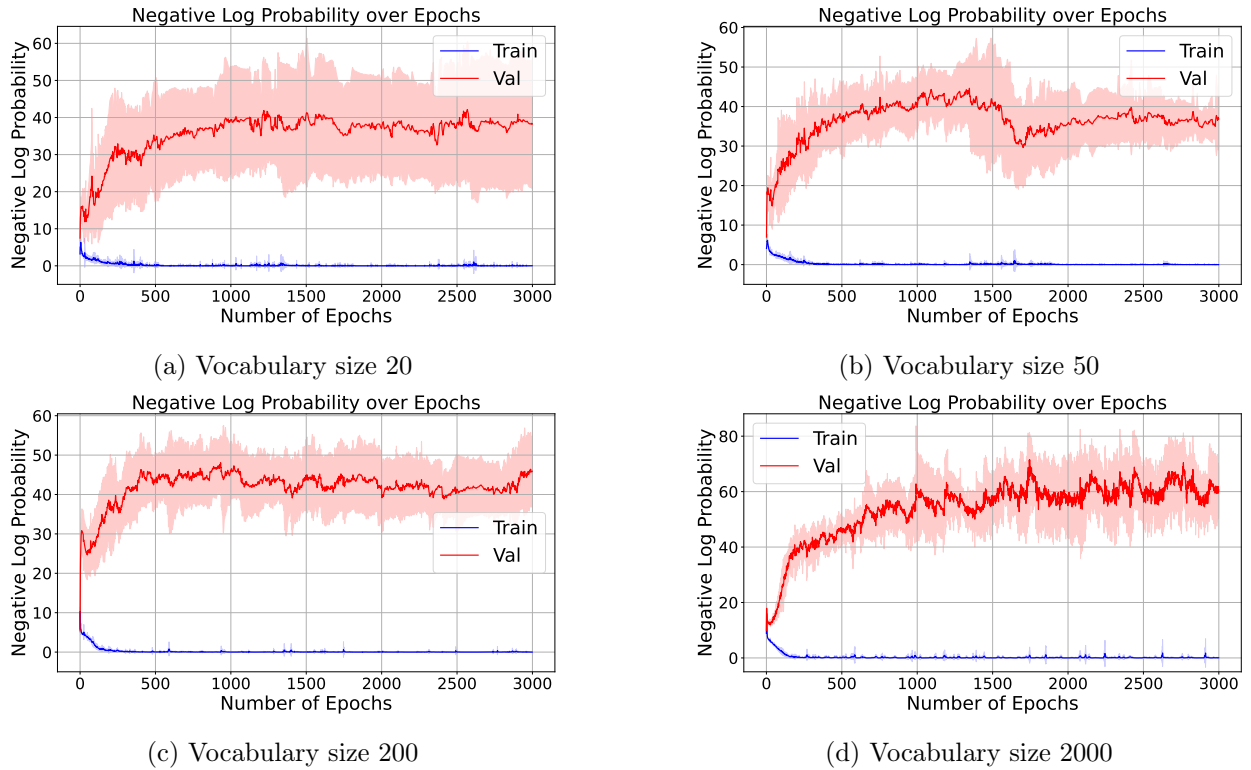
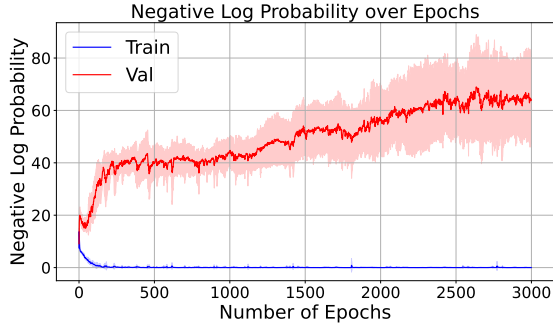
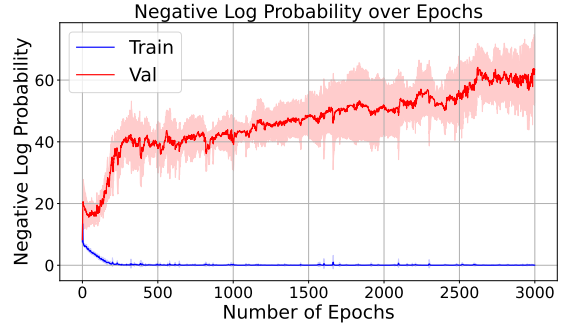


Figure 5: Results for reversal curse for different vocabulary sizes. All other configurations are set as default values as in [Table 3](#). The training set sizes for the above four experiments are 9, 20, 85, 850 respectively, and the validation set sizes are 1, 4, 15, 150 respectively.

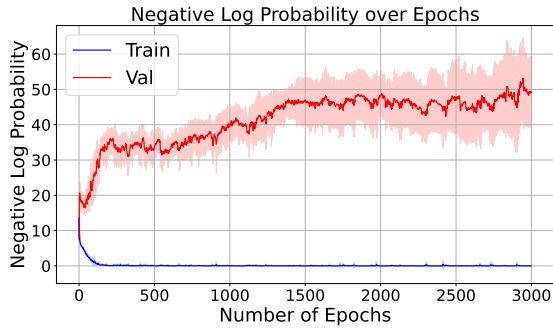


(a) 12 layers

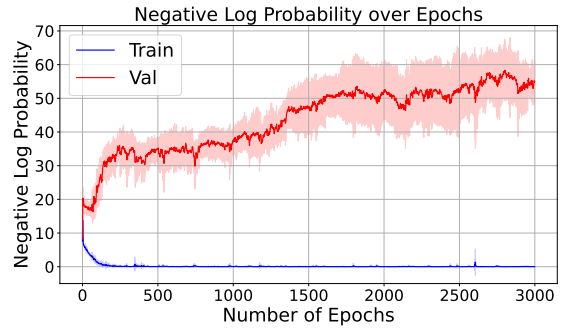


(b) 48 layers

Figure 6: Results for reversal curse for different numbers of layers of the transformer. All other configurations are set as default values as in Table 3.

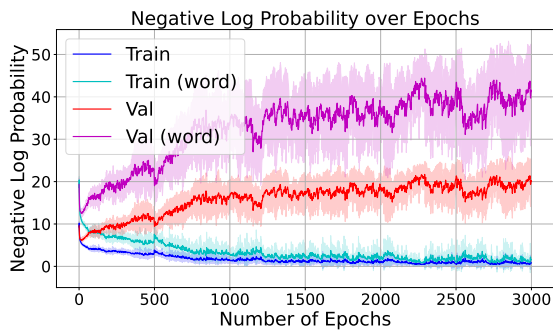


(a) No positional encoding

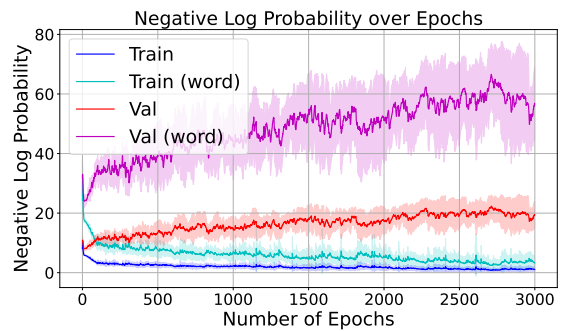


(b) Relative positional encoding

Figure 7: Results for reversal curse with no positional encoding or relative positional encoding. For relative positional encoding, we follow the Rotary Position Embedding (RoPE) method proposed by Su et al. (2024). All other configurations are set as default values as in Table 3.



(a) Entity length 2



(b) Entity length 3

Figure 8: Results for reversal curse with different entity lengths. Each entity A_i , B_i or C_i consists of multiple tokens and different entities may have overlapped tokens. The “Train” curve represents the negative log probability of predicting the first token of the output entity, and “Train (word)” represents the negative log probability of predicting all tokens one by one of the output entity. All other configurations are set as default values as in Table 3. The training set sizes for the above two experiments are 680 and 250, respectively, and the validation set sizes are 120 and 50, respectively.

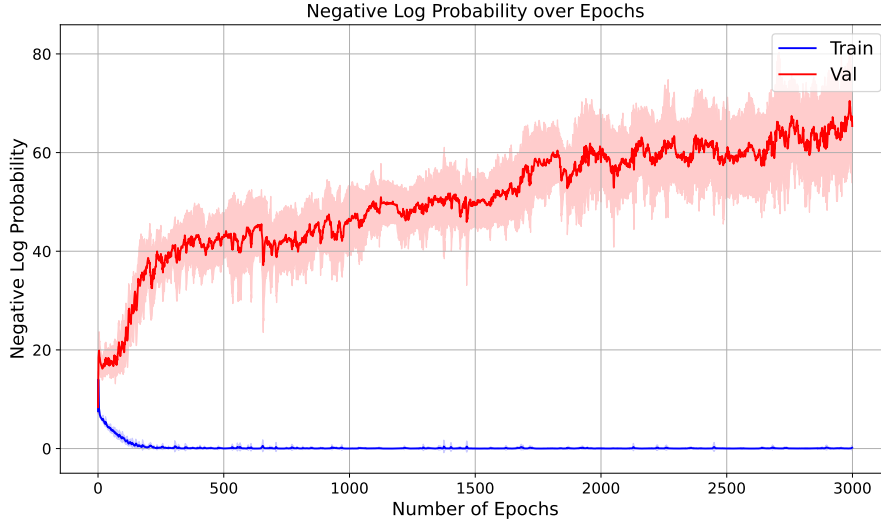


Figure 9: Results for reversal curse with fixed token embedding and fixed positional embedding. All other configurations are set as default values as in Table 3.

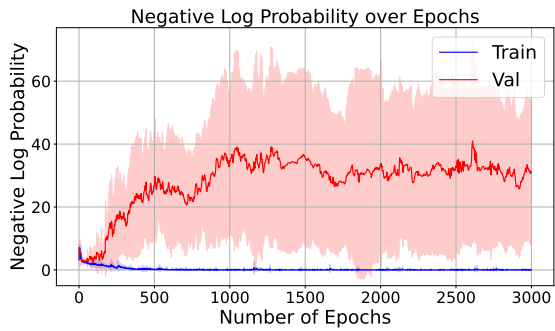
C.3 Additional experimental results for chain-of-thought

In this section, we show additional experimental results for COT under different configurations, including different vocabulary sizes (Figure 10), different number of layers (Figure 11), different positional encoding (Figure 12), different entity lengths (Figure 13) and whether token and positional embeddings are trainable or fixed (Figure 14). Note that our experimental results consistently show the necessity of COT under different settings.

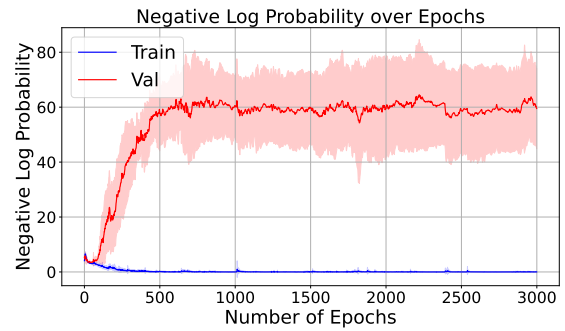
C.4 Chain-of-thought with relevant tokens

In Section 5.2, we briefly mentioned that the irrelevance of different entity tokens is one of the reasons that COT is necessary. Now, we show that if the entity tokens are correlated and show specific patterns, it is possible for a model to deduce indirect implications automatically.

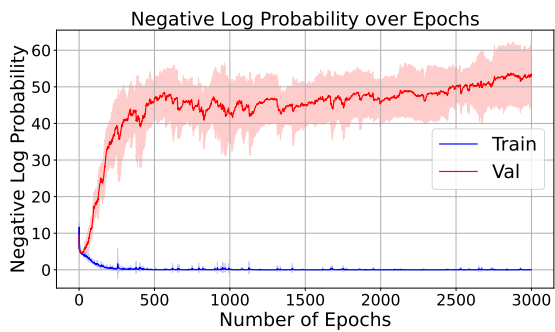
Instead of using single tokens A_i, B_i, C_i to represent each entity, now we use two tokens A_i, B_i, C_i to represent entities, where A, B and C are three common tokens shared by each triple, and token i are distinct for each triple. Figure 15 shows that for the above version of COT where tokens in the same chain are correlated, the model is able to “deduce” $A_i \rightsquigarrow C_i$ after training on $A_i \rightarrow B_i, B_i \rightarrow C_i$ and other training samples.



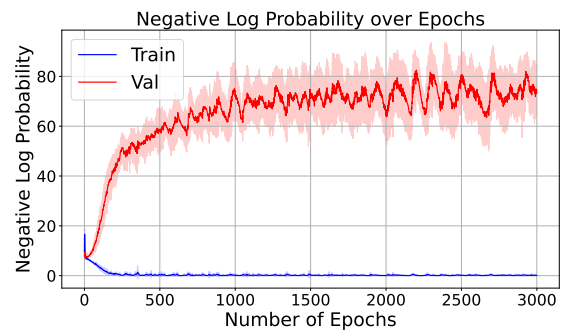
(a) Vocabulary size 20



(b) Vocabulary size 50

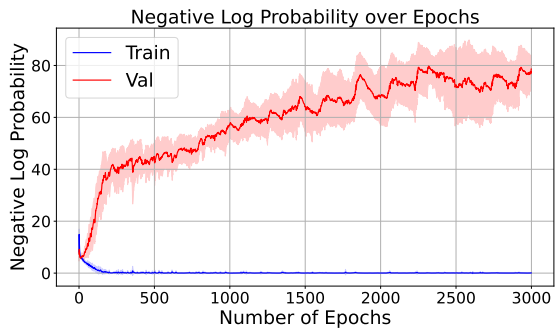


(c) Vocabulary size 200

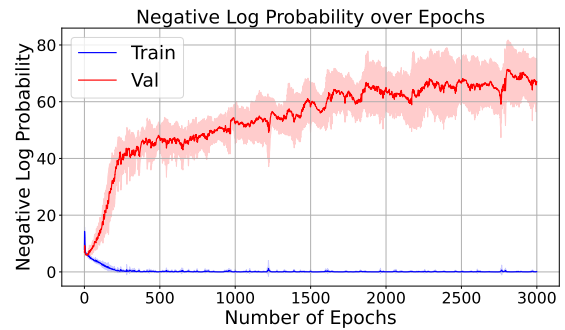


(d) Vocabulary size 2000

Figure 10: Results for COT for different vocabulary sizes. All other configurations are set as default values as in Table 3. The training set sizes for the above four experiments are 14, 32, 135, 1350 respectively, and the validation set sizes are 1, 4, 15, 150 respectively.

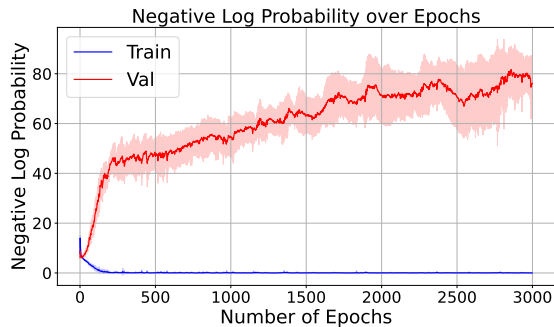


(a) 12 layers

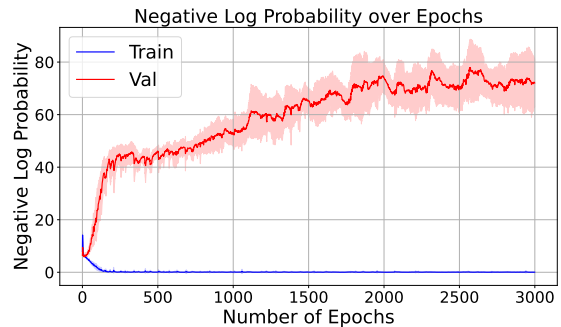


(b) 48 layers

Figure 11: Results for COT for different number of layers of the transformer. All other configurations are set as default values as in Table 3.

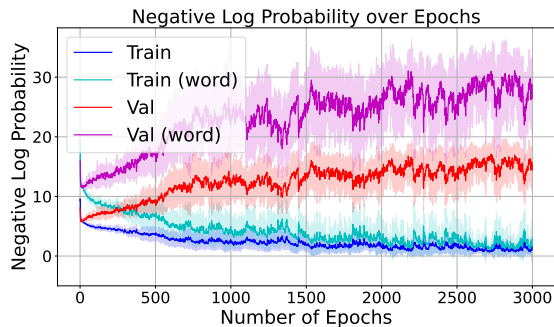


(a) No positional encoding

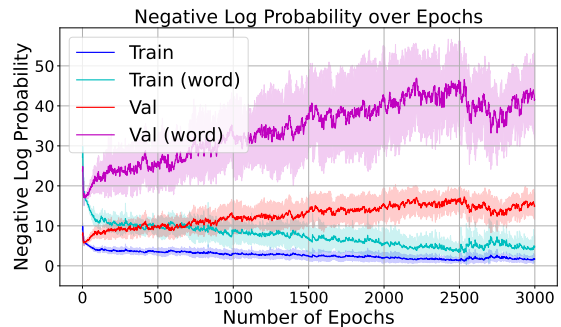


(b) Relative positional encoding

Figure 12: Results for COT with no positional encoding or relative positional encoding. For relative positional encoding, we follow the Rotary Position Embedding (RoPE) method proposed by [Su et al. \(2024\)](#). All other configurations are set as default values as in [Table 3](#).



(a) Entity length 2



(b) Entity length 3

Figure 13: Results for COT with different entity lengths. Each entity A_i, B_i consists of multiple tokens and different entities may have overlapped tokens. The “Train” curve represents the negative log probability of predicting the first token of the output entity, and “Train (word)” represents the negative log probability of predicting all tokens one by one of the output entity. All other configurations are set as default values as in [Table 3](#). The training set sizes for the above two experiments are 1080 and 400, respectively, and the validation set sizes are 120 and 50, respectively.

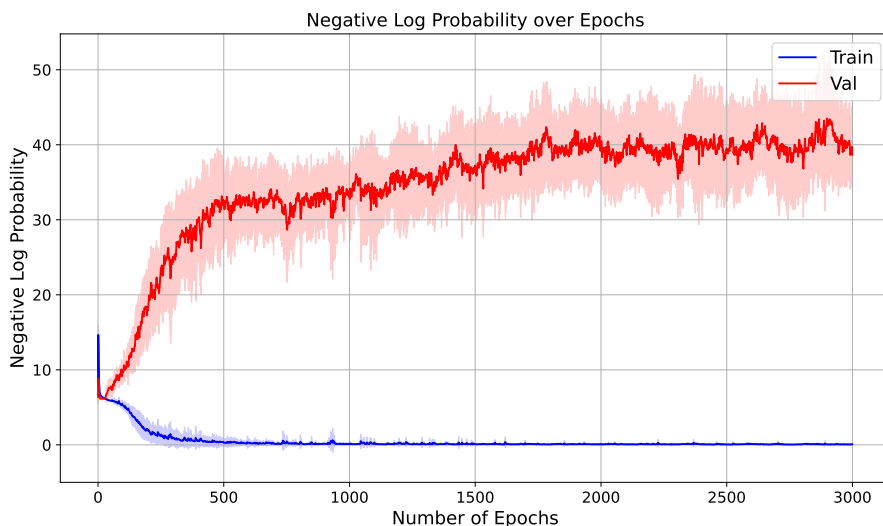
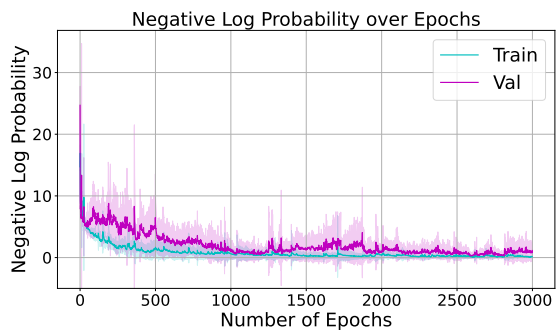
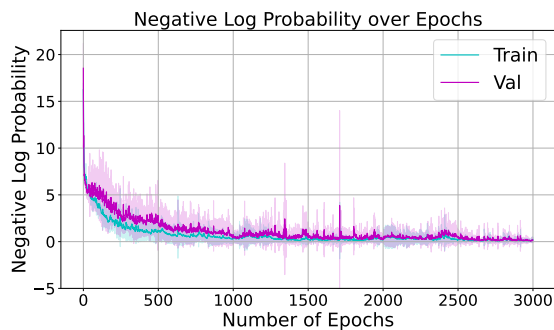


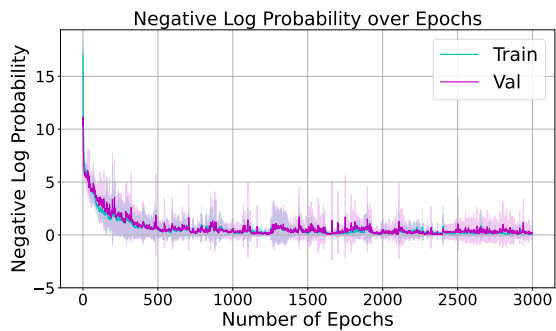
Figure 14: Results for COT with fixed token embedding and fixed positional embedding. All other configurations are set as default values as in Table 3.



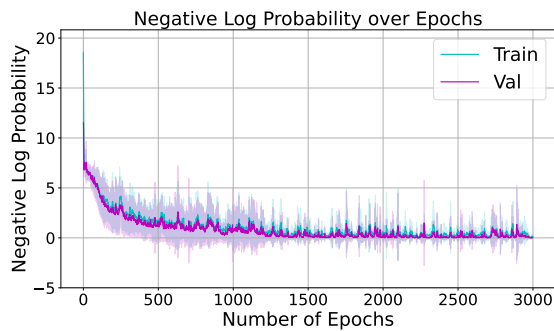
(a) Training set size 160



(b) Training set size 250



(c) Training set size 400



(d) Training set size 1600

Figure 15: Results for COT where each entity is represented by two tokens, i.e., A_i , B_i , or C_i . The validation set sizes are 50. The model is able to “deduce” unseen $A_i \rightsquigarrow C_i$ by “cheating” since the model can directly learn the pattern of entity tokens.